Monitoring Lung Volumes During Mechanical Ventilation

14

Educational Goals

This chapter aims to describe:

- The theoretical basis and technique of RIP
- The measurement of tidal volume and changes in end-expiratory lung volume during mechanical ventilation using RIP, including the limitations of these measurements
- The potential applications for RIP in neonatal and paediatric intensive care, including during high-frequency ventilation and newborn resuscitation

This chapter will not discuss the use of RIP within the field of sleep medicine.

14.1 Respiratory Inductive Plethysmography

David Tingay and Peter A. Dargaville

14.1.1 Introduction

Respiratory inductive plethysmography (RIP) is a non-invasive method of measuring change in lung volume which is well-established as a monitor of tidal ventilation and thus respiratory patterns in sleep medicine. As RIP is leak independent, can measure end-expiratory lung volume as well as tidal volume and is applicable to both the ventilated and spontaneously breathing patient, there has been recent interest in its use as a bedside tool in the intensive care unit.

14.1.2 Technique

14.1.2.1 Theoretical Considerations

RIP determines change in lung volume by measuring the changes in both chest and abdominal volume displacements during tidal ventilation. In 1967, Konno and Mead, using the principle that there is a relationship between linear motion and volume displacement, showed that the chest wall operates with 2° of freedom and has two moving parts, the rib cage and the abdomen (Konno and Mead 1967). Additionally, in terms of motion of their surfaces, there is functional separation between the abdomen and the rib cage during

P.C. Rimensberger (ed.), *Pediatric and Neonatal Mechanical Ventilation*,
DOI 10.1007/978-3-642-01219-8_14, © Springer-Verlag Berlin Heidelberg 2015

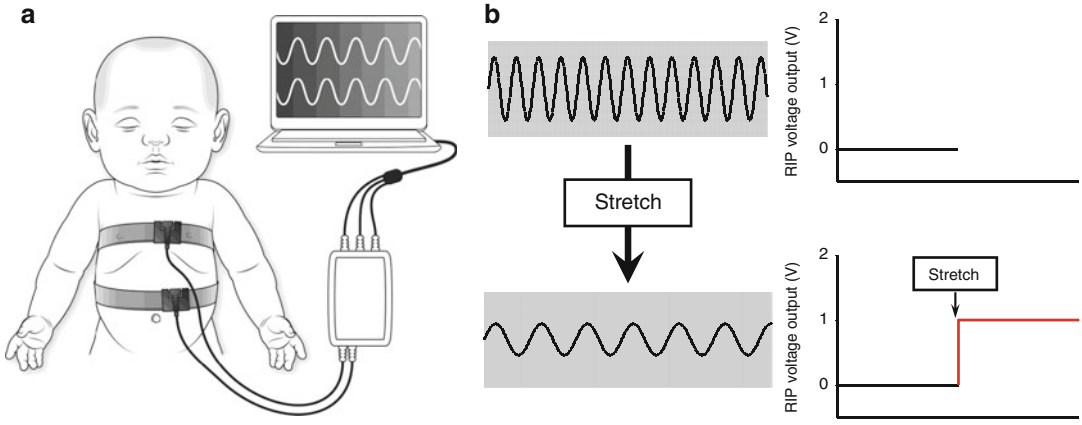

Fig. 14.1 (**a**) Illustration of RIP transducer bands correctly secured around the chest and abdomen of an infant. A sinusoidal wire embedded is in each band. (**b**) Schematic illustration of the relationship between changes in RIP voltage output (V) generated by stretch of the sinusoidal wire secondary to change in lung volume

breathing. By utilising this unitary behaviour of the two compartments, change in total thoracic volume[1] can be determined from measurement of the volume displacement in each separate compartment. During ventilation, the lung will contribute to the majority of any thoracic volume change.

Thus, lung volume (V_L) can be mathematically expressed as follows:

$$V_L = V_{Lch} + V_{Lab} \qquad (14.1)$$

where V_{Lch} and V_{Lab} represent volume displacement within the chest and abdominal compartments, respectively.

The true practical advantage of Konno and Mead's observation can be realised by considering the fact that a volume change will result in a change in cross-sectional area within each compartment.

Hence, V_L can be considered as

$$V_L = m\left(k \times \Delta R_{ch} + \Delta R_{ab}\right) \qquad (14.2)$$

where R_{ch} and R_{ab} are the cross-sectional areas of the chest and abdomen compartments respectively, k is a proportionality constant, representing the relative contribution of each compartment to total volume, and m scales the sum of the cross-sectional areas to a known volume (Sackner et al. 1989; Bar-Yishay et al. 2003).

[1]Total thoracic volume is the combined volume of gas, blood and tissue within the thoracic cavity.

14.1.2.1.1 Equipment

RIP systems employ two transducers, placed circumferentially around the chest and abdomen, to measure changes in the cross-sectional area of each (Watson et al. 1988; Adams 1996). Each transducer consists of a sinusoidal wire embedded in an elastic self-adherent material (Fig. 14.1). This allows the transducers to be applied to any chest or abdominal shape and size. One band is usually placed at nipple level (R_{ch}) and the other approximately 1 cm above the umbilicus (R_{ab}). These wires are connected to an electronic oscillator that generates a sine wave of 20 mV at 300 kHz. Stretch and relaxation of the bands produce variations in the electrical self-inductance within the wire and, thus, frequency (Adams 1996). The RIP unit demodulates the frequency change to produce an analogue voltage waveform representing the changes in rib cage and abdominal volume in real time (Ohms Law). The inductance within the wires increases linearly as a function of cross-sectional area in curved-shaped objects (Watson et al. 1988; Martinot-Lagarde et al. 1988; Brazelton et al. 1999a). The output of RIP is reliable within the frequency range of both conventional and high-frequency ventilator rates (Brazelton et al. 1999a, b; Boynton et al. 1989).

Early RIP devices operated solely in AC-coupled output mode. This was adequate for assessing respiratory rate, tidal volume and synchrony of respiration, but the baseline signal was too unstable to assess end-expiratory lung volume (EELV) (Morel et al. 1983). Modern RIP devices allow both an AC- and DC-coupled output. In DC-coupled output, the RIP signal is sufficiently stable to allow reliable measurement of changes in EELV (Morel et al. 1983; Valta et al. 1992a), with good agreement with EELV values obtained by whole-body plethysmography (Carry et al. 1997) and super-syringe (Albaiceta et al. 2003).

14.1.2.1.2 Calibration

Changes in lung volume recorded by RIP are initially output as voltage changes. The RIP voltage change can be calibrated using a number of methods (Bar-Yishay et al. 2003). The two most common are the qualitative diagnostic calibration (QDC) algorithm (Sackner et al. 1989) and the least mean squares technique (Konno and Mead 1967; Strömberg et al. 1993). The least mean squares technique requires knowledge of a known volume change during the calibration phase, which is not always possible during paediatric and neonatal ventilation. For this reason, the QDC algorithm is the method most commonly used in ICU environments.

The QDC measures the voltage changes during a series of breaths at the start of the RIP recording, generally over 5 min. QDC allows derivation of the proportionality constant, k, in Eq. 14.2. The relative contribution of each compartment to the overall voltage change is estimated by selecting a series of breaths of similar tidal volume. This is achieved by excluding all breaths greater than one standard deviation (SD) of the mean ΔR_{ch} and ΔR_{ab} value. The constant k is then estimated as $SD(R_{ch})/SD(R_{ab})$ (Sackner et al. 1989). QDC has been shown to generate acceptable agreement with pneumotachograph measurement of tidal volume in term newborn infants (Adams 1996) and piglet models of surfactant-deficient lung disease (Markhorst et al. 2006). The reliability of RIP calibration is best when measurements are immediately preceded by calibration and tend to deteriorate with time. RIP calibration accuracy decreases with severity of lung disease. In vitro, the phase deviation in the transducer outputs, and thus the stability of the proportionality factor, increases in a linear fashion at frequencies above 10 Hz (Boynton et al. 1989). The accuracy of this process is also directly related to the number of breaths analysed (Brown et al. 1998).

If the volumetric changes during the QDC are known, for example, using a pneumotachograph or super-syringe, then the scaling factor, m, can be determined for Eq. 14.2, and the RIP signals displayed in units of volume (Fig. 14.2). Calibration and signal stability can then be maintained if the band location and tension remain constant and the patient's position, or pattern of breathing, does not change (Landon 2002).

An advantage of the QDC method is that it can still be applied when absolute volume changes are not known. In these circumstances, changes in relative volume can be expressed as a ratio to the tidal volume during the QDC period. This is useful during non-invasive ventilation (Courtney et al. 2001) and high-frequency ventilation (Markhorst et al. 2006; Habib et al. 2002; Weber et al. 2000; Markhorst and van Genderingen 2004; Copnell et al. 2009; Hoellering et al. 2008; Tingay et al. 2006, 2007a). After QDC, a modern RIP device has been found to have a mean relative measurement bias of −2.0 (SD 9 %) during short periods of high-frequency ventilation (HFV) in a piglet model of paediatric lung disease (Markhorst et al. 2006; Markhorst and van Genderingen 2004). This error is less than common commercially available pneumotachographs (Scalfaro et al. 2001; Roske et al. 1998). This study also demonstrated that a k factor of 1.0 was reasonable for most paediatric lung disease states, overcoming some of the difficulties associated with QDC during high-rate, low tidal volume ventilation.

14.1.2.2 Clinical Applications

14.1.2.2.1 Assessment of EELV

The capacity of DC-coupled output RIP to achieve a stable baseline signal offers the potential to reliably measure change in EELV during mechanical ventilation, particularly high-

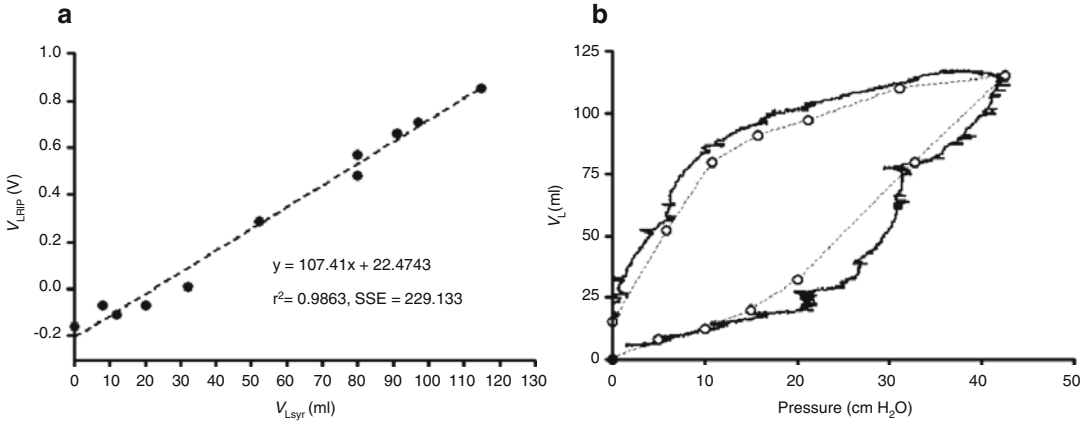

Fig. 14.2 (**a**) Relationship between super syringe volume (V_{Lsyr}) and RIP (V_{LRIP}) during a static pressure-volume curve between 0 and 40 cm H_2O in a preterm lamb. RIP demonstrates a strong correlation over a wide range of lung volumes. (**b**) Resultant pressure-volume relationship after calibrating the RIP unit (*solid lines*). *Open circles*; Pressure – V_{Lsyr} relationship

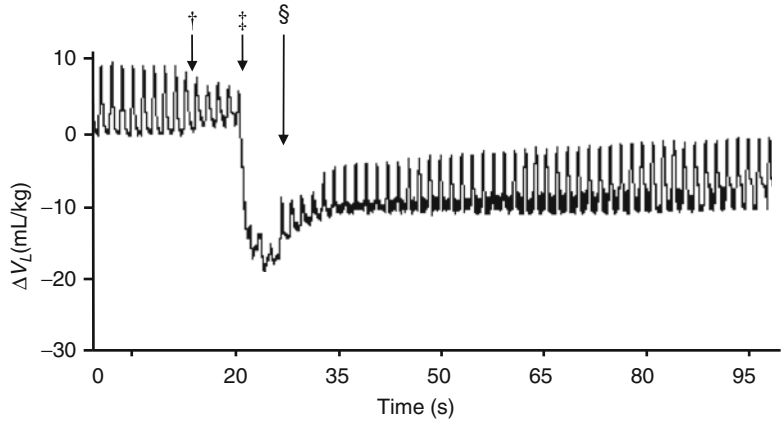

Fig. 14.3 Change in lung volume during endotracheal tube suction using a closed technique in an animal model of paediatric lung disease demonstrating the ability of RIP to document changes in both EELV and V_T. Insertion of the suction catheter into the endotracheal tube (†), ‡ application of negative pressure suction and § completion of suction process (Adapted from Copnell et al. (2009). Reproduced with permission © 2009 International Pediatric Research Foundation, Inc)

frequency and non-invasive ventilation. Most modern ventilators include continuous airway flow monitoring, allowing RIP to be calibrated easily and frequently during conventional forms of mechanical ventilation.

14.1.2.2.1.1 Conventional Mechanical Ventilation

The first use of RIP to measure EELV was in an adult population after open heart surgery (Valta et al. 1992a, b). In this study, RIP was successfully used to measure the ΔEELV at different PEEP levels. This suggests that RIP may have potential to define an optimal PEEP during conventional mechanical ventilation in the paediatric population. RIP has frequently been used to measure ΔEELV during endotracheal tube suction (Copnell et al. 2009; Hoellering et al. 2008; Choong et al. 2003) (Fig. 14.3). In these studies, RIP has been able to accurately identify small changes in absolute and relative ΔEELV in infants and children ventilated with (Choong et al. 2003) and without (Hoellering et al. 2008) muscle relaxants.

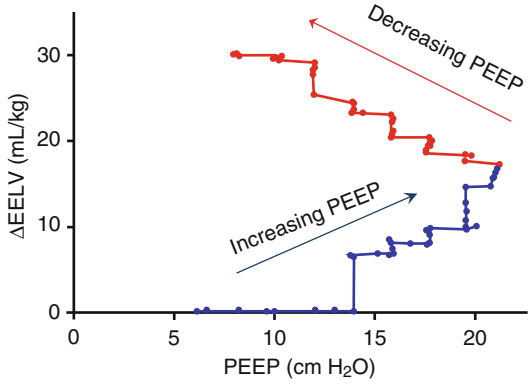

Fig. 14.4 Change in end-expiratory lung volume (mL/kg) during step-wise changes in PEEP in a preterm lamb. Ventilation applied using positive-pressure ventilation with a targeted tidal volume of 7 mL/kg

To date, there are no reports of the use of RIP as a guide to the optimal application of PEEP in the paediatric population, despite the potential RIP offers in this field. Pilot data in preterm lambs suggest that RIP can map ΔEELV very effectively during conventional mechanical ventilation (Fig. 14.4).

14.1.2.2.1.2 High-Frequency Ventilation

RIP has found a place in measurement of lung volume during high-frequency ventilation (HFV), in large part due to the difficulties in assessing volumetric change with other devices. The non-laminar gas flow during HFV makes pneumotachographic measurement of tidal volume difficult and measurement of EELV impossible (Gerstmann et al. 1990). RIP measures volume change directly within the thoracic cavity and is unaffected by flow characteristics. RIP thus has the potential to measure both tidal volume and EELV during HFV.

Calibrated RIP has been used to measure changes in lung volume during endotracheal tube suction in a small population of infants receiving HFV (Tingay et al. 2007a). This was achieved by calibrating the RIP voltage change against tidal volume at the airway opening in a series of tidal inflations during conventional ventilation. This technique requires transient discontinuation of HFV and, possibly, disconnection from mechanical ventilation. It is reasonable to conclude that this method of calibration would be accurate for short periods during HFV. Whether the calibration factors remain accurate over longer periods is questionable, especially in states of severe, or changing, lung disease (Tingay et al. 2007b).

Even when uncalibrated, RIP still has clinical potential to measure relative changes in lung volume during HFV and avoids the limitations of calibration (Markhorst et al. 2006). On the benchtop, uncalibrated RIP accurately measures relative change in EELV during HFV between frequencies of 7 and 15 Hz (Brazelton et al. 1999a), with a stable signal for up to 4 h in a thermally constant environment (Brazelton et al. 1999b). Signal stability beyond 3 h has not been confirmed in human studies (Tingay et al. 2006).

Uncalibrated RIP has been shown to be a reliable method of assessing relative change in EELV during HFV in animal models of neonatal lung disease, agreeing with changes in lung volume measured using whole-body plethysmography (Weber et al. 2000), super-syringe-derived pressure-volume relationships (Brazelton et al. 2001; Gothberg et al. 2001) and single-slice chest computed tomography (Authors' unpublished data).

The first reported use of RIP to record changes in EELV during HFV was by Saari et al. (1984) in which dynamic hyperinflation was demonstrated in seven adult patients receiving high-frequency ventilation. More recently, RIP has been used to describe the relationship between applied P_{aw} and thoracic volume during HFV in animal models of surfactant-deficient lung disease. Identification of lung overdistension during sequential increases in P_{aw} was possible in the healthy and surfactant-depleted piglet lung using RIP-derived static compliance (Weber et al. 2000). In both lung models, the relationship between applied P_{aw} and compliance fitted a second-order sigmoidal model of the pressure-volume relationship (Venegas et al. 1998), with the P_{aw} resulting in overdistension translating to the upper inflection point of the sigmoid curve, suggesting that RIP could be used to describe the inflation limb of the pressure-volume relationship (Weber et al. 2000). The same group has also shown that RIP-derived time constants of the lung can be used to identify the point of optimal

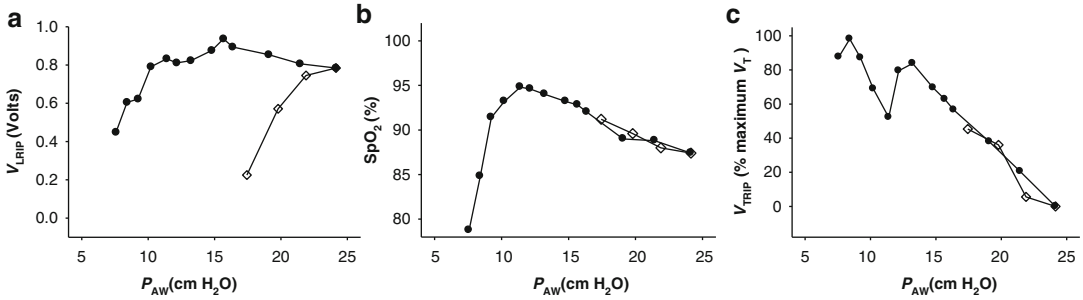

Fig. 14.5 (**a**) Relationship between mean airway pressure (P_{AW}) and EELV, measured with RIP (V_{LRIP}) during an open lung recruitment strategy in a muscle-relaxed term infant receiving HFOV for meconium aspiration syndrome. Open lung recruitment strategy consisted of a series of step-wise increases in P_{AW} (*open diamonds*) until total lung capacity, followed by step-wise decreases (*closed circles*) until the closing pressure of the lung was identified by persistent desaturation (**b**). (**c**) Relationship between HFOV tidal volume, measured by RIP (V_{TRIP}) and normalised to the maximum V_{TRIP} identified, during the same open lung recruitment strategy

ventilation during sequential P_{aw} increases (Habib et al. 2002).

Increasingly, strategies which aim to apply HFV at the lowest possible P_{aw} that maintains lung volume after a recruitment manoeuvre are being advocated (Rimensberger et al. 1999a, b, 2000a, b; van Kaam and Rimensberger 2007; De Jaegere et al. 2006; van Kaam et al. 2003, 2004a, b; Lachmann 1992; Vazquez de Anda et al. 1999, 2000; Froese 1997). Mapping the volumetric response to recruitment is difficult at the bedside, and clinicians are limited to resorting to indirect indicators of lung volume, such as oxygenation. In a piglet model of paediatric acute respiratory distress syndrome (Brazelton et al. 2001) and term and preterm lambs (Gothberg et al. 2001), RIP has been used to demonstrate lung volume recruitment, hysteresis and subsequent optimal P_{aw} on the deflation limb of the pressure-volume relationship of the lung. In both these studies, critical points within the pressure-volume relationship, including total lung capacity, were identifiable. RIP can also demonstrate improvement in the hysteresis of the lung after administration of exogenous surfactant (Gothberg et al. 2001).

RIP has been used to map relative lung volume changes during an open lung recruitment strategy in 15 term to near-term muscle-relaxed infants receiving HFV (Tingay et al. 2006). RIP was used to determine the relationship between EELV and applied pressure, oxygenation and lung mechanics (Fig. 14.5). For the first time, lung recruitment, hysteresis and the closing pressure of the lung could be identified during HFV in infants. In addition, a direct relationship between oxygenation and lung volume was confirmed. This study demonstrated that uncalibrated RIP could be reliably used over prolonged periods (up to 3 h) to track ΔEELV. Subsequently, the authors were able to demonstrate that RIP could determine the time when stable EELV had been achieved after a pressure change (Tingay et al. 2005).

14.1.2.2.1.3 Non-invasive Ventilation

Similar to HFV, application of non-invasive ventilation is to some extent hampered by a lack of reliable direct measures of lung volume. Despite the increasingly popularity of non-invasive modes of ventilation to treat neonatal and paediatric lung disease, a strategy to define optimal continuous distending pressure (CDP) remains elusive. Interestingly, the use of RIP to measure EELV during CPAP is limited to two studies in preterm infants (Courtney et al. 2001; Elgellab et al. 2001). In both studies, RIP was able to track the relationship between PEEP and EELV during a series of PEEP changes from 0 to 8 cm H_2O. One study measured relative ΔEELV using the RIP-determined V_T value as a unit of volume (Elgellab et al. 2001). The other calibrated the RIP signal to the pneumotachograph V_T during a brief period of spontaneous breathing through a face mask (Courtney et al. 2001), a technique that has been validated previously (Brooks et al. 1997). Both

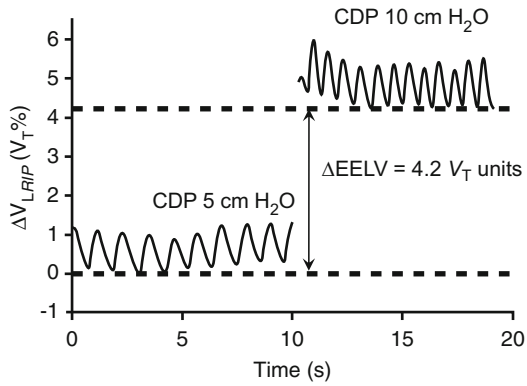

Fig. 14.6 Uncalibrated RIP tracing in a preterm infant receiving CPAP at a continuous distending pressure (*CDP*) of 5 cm H_2O and 10 cm H_2O. RIP is able to demonstrate tidal volume, respiratory rate and change in end-expiratory lung volume (**Δ**EELV). RIP units expressed as a proportion of the average tidal volume during the 5 cm H_2O tracing

calibration techniques would be clinically reproducible. The results of both these studies suggest that RIP may be useful in determining the optimal CDP during CPAP (Fig. 14.6).

14.1.2.2.2 Assessment of Tidal Volume and Breathing Patterns

The first use of RIP to assess tidal breathing patterns in spontaneously breathing infants was described by Duffty et al. (1981). Since then, RIP has been used extensively to assess tidal volume, thoraco-abdominal asynchrony and work of breathing in infants (Strömberg et al. 1993; Courtney et al. 2001; Habib et al. 2002; Dolfin et al. 1982; Tabachnik et al. 1981; Stefano et al. 1986; Adams and Zabaleta 1993a, b, 1994). These initial studies demonstrated the accuracy of RIP in measurement of V_T, in calibrated and uncalibrated modes, even over long periods of time (Brooks et al. 1997). The accuracy of RIP compared favourably with impedance sensors and strain gauges (Adams and Zabaleta 1993b). Apart from a direct measure of tidal volume, RIP allows the potential to assess the respiratory effort and pattern over time. As RIP is a measure of chest wall and abdominal movement, detection of apnoea is possible (Brooks et al. 1997; Weese-Mayer et al. 2000). During spontaneous breathing, knowledge of the synchrony of the abdominal and thoracic compartments is important as the summated signal constitutes the measured tidal volume. If the two compartments are out of phase (paradoxical breathing), there is the potential for the summated time course signal to indicate no tidal ventilation (Fig. 14.7). Such states of significant asynchrony of thoraco-abdominal motion signify poor lung mechanics and lead to significant diaphragmatic work and fatigue (Musante et al. 2001; Schulze et al. 2001; Guslits et al. 1987).

14.1.2.2.2.1 Conventional Mechanical Ventilation

Due to the availability, relative ease and reliability of pneumotachographic assessment of tidal volume at the airway opening, there are very few reports of assessment of tidal volume using RIP during conventional mechanical ventilation. RIP has been used to identify improved tidal volume, thoraco-abdominal synchrony and chest wall displacement after transition to proportional assist ventilation from CPAP (Musante et al. 2001).

RIP has been shown to be a reliable alternative to pneumotachography in driving ventilator synchronisation during conventional mechanical ventilation in animal models of the normal and diseased paediatric lung (Schulze et al. 2001). The accuracy of the RIP bands was depended on a reliable calibration of the contribution of each band to the summated signal. This accuracy diminished significantly after body movement, limiting the use of the summated signal for prolonged mechanical ventilation periods in ICU. Schulze et al. have proposed that the use of the abdominal band alone would overcome these difficulties and offer the advantage of being a leak- and dead-space-free method of determining spontaneous respiratory effort (Schulze et al. 2001).

Pneumotachography will be unreliable during states of rapid compliance change or respiratory asynchrony, such as endotracheal tube suction (Copnell et al. 2009; Hoellering et al. 2008) and surfactant administration. During these situations, RIP is likely to be a better indicator of tidal volume change in the thorax.

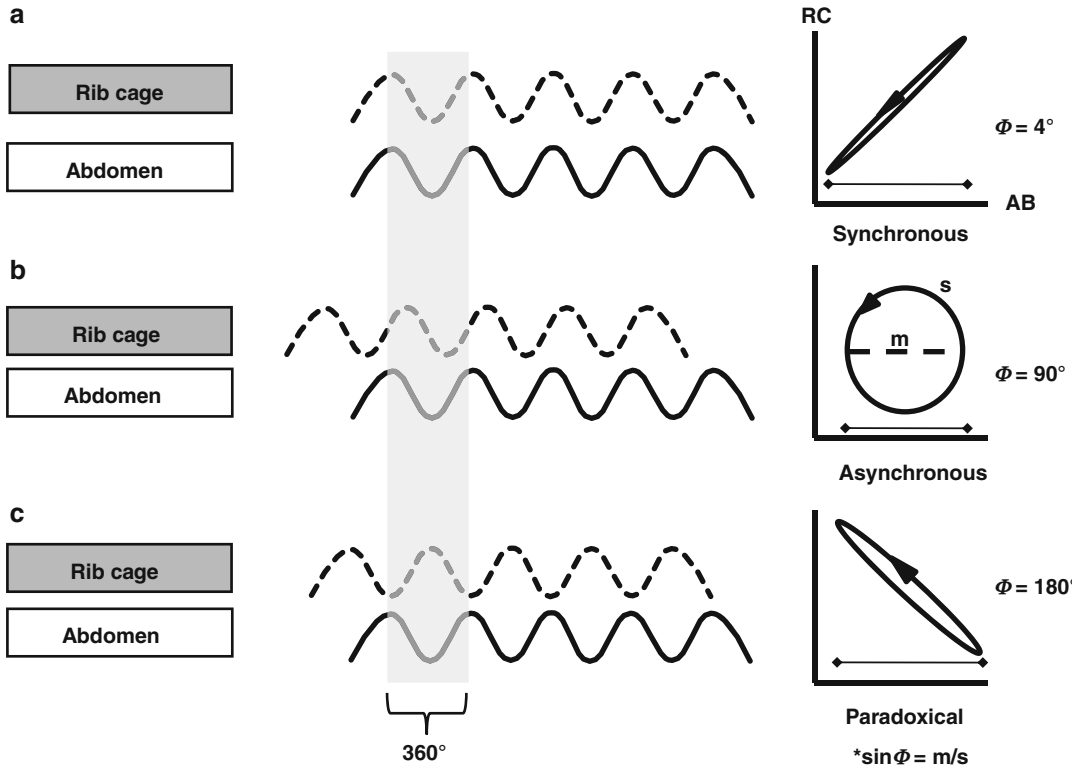

Fig. 14.7 RIP waveforms during tidal ventilation to illustrate synchronous (in phase; **a**), asynchronous (**b**) and paradoxical (completely out of phase; **c**) patterns of thoraco-abdominal motion. The resultant Lissajous plot (Konno-Mead plot) of rib cage (*RC*) against abdomen (*AB*) displacement during a single breath (highlighted in *grey*) shown on the *right*. Phase angles of 0° indicate perfectly synchronous thoraco-abdominal motion and 180° completely asynchronous motion. Poor lung mechanics and respiratory muscle fatigue is associated with highly asynchronous states (Figure courtesy of Dr Christopher Newth)

14.1.2.2.2.2 High-Frequency Ventilation

Assessment of V_T during HFV is problematic. Pneumotachographic measures at the airway opening provide an accurate trend of HFV V_T in vitro (Scalfaro et al. 2001), but do not correspond with the volumetric changes measurable at the chest wall. The accuracy of pneumotachography during HFV in humans has not been confirmed (Zimova-Herknerova and Plavka 2006); thus, it should be considered at best a proxy for tidal changes more distally in the tracheobronchial tree. In contrast, RIP is a direct measure of chest wall movement during HFV and likely to be a better representative of tidal volume. In an animal model of paediatric acute lung injury, RIP tidal amplitudes could be accurately measured and altered accordingly with changing PEEP and compliance (Markhorst et al. 2005, 2006). RIP tidal amplitude could then be used to identify overdistension during HFV. A similar relationship between volume state of the lung and RIP-derived V_T has been found in human infants receiving HFV (Fig. 14.5) (Tingay 2013). In this study, the RIP-derived V_T response approximated that of V_T measured by pneumotachograph (Tingay 2008).

14.1.2.2.2.3 Non-invasive Ventilation

The early descriptions of RIP in infants related to tidal patterns in spontaneously ventilated subjects (Strömberg et al. 1993; Duffty et al. 1981; Dolfin et al. 1982; Stefano et al. 1986). Compared to pneumotachography, RIP shows good agreement as a measure of V_T during CPAP and spontaneous ventilation in preterm infants (Bar-Yishay et al. 2003; Brown et al. 1998). Unlike face mask

pneumotachography, RIP offers the ability to monitor tidal ventilation without significant disruption and can determine the synchrony of ventilation using the phase angle between the chest and abdominal tidal signals, sometimes expressed as a laboured breathing index (LBI). RIP has been used to demonstrate the effect of alterations in continuous distending pressure on tidal breathing patterns in preterm infants receiving CPAP. A higher pressure (maximum 8 cm H_2O) resulted in a better V_T and thoraco-abdominal synchrony and lower LBI, suggesting less work of breathing (Elgellab et al. 2001). Courtney and co-workers also demonstrated an association between increased respiratory rate and greater phase angle with CPAP delivered via nasal cannulae compared with short binasal prongs (Courtney et al. 2001). These small studies suggest that RIP may be useful as a monitoring device during CPAP.

14.1.2.3 Limitations

The most important limitation of RIP is the inability to determine the residual volume of the lung and absolute volume change. Furthermore, change in inductance measured by RIP is linearly related to total thoracic volume rather than gas volume per se. We have noted that RIP detects blood volume change within the chest during intravenous administration of fluid boluses (Authors unpublished data).

Early RIP systems were also susceptible to significant thermal drift, limiting the capacity to accurately monitor ΔEELV (Bhatia et al. 2010). Some modern RIP devices require up to 60 mins to achieve signal stability in a stable ambient temperature (Tingay 2008; Bhatia et al. 2010), but thereafter, signal stability is excellent and, in many cases, better than pneumotachographs (Markhorst et al. 2006; Brazelton et al. 2001; Tingay 2008). Drift appears to be less of an issue in newer RIP systems (Bhatia et al. 2010). The disease state of the lung may also affect the drift of the RIP signal. RIP was found to be unreliable during mechanical ventilation in adults with severe obstructive pulmonary disease (Neumann et al. 1998; Werchowski et al. 1990).

Strict adherence to a standardised method of transducer placement is required to reduce intersubject variability (Landon 2002). The chest and abdomen are most likely to operate with 1° of freedom when transducers are placed at the level of the nipples and at, or just above, the umbilicus (Konno and Mead 1967; Tingay et al. 2006; Brooks et al. 1997; Weese-Mayer et al. 2000). Most reports of RIP during paediatric critical care have equally weighted the chest and abdominal contributions. There is some evidence to support this assumption in paediatric acute lung injury (Markhorst et al. 2006), although it should be noted that this assumption is not universally true and may significantly alter measurement error (Poole et al. 2000).

The greatest hindrance for RIP is the lack of commercially available products specifically for intensive care use. Until RIP devices that measure changes in EELV and V_T are integrated into modern monitoring systems, the potential for RIP is limited to a research tool.

14.1.2.4 Future Directions

The use of RIP in the resuscitation of newborn infants has not been described. Birth is a time of significant volume change in the lung. Increasingly, the need to establish adequate aeration is being recognised. Theoretically, RIP may offer promise in this clinical environment. Preliminary data in animal models of prematurity show that RIP can demonstrate tidal and end-expiratory lung volume change during resuscitation at birth (Fig. 14.8). As bedside lung mechanics monitors incorporating airway flow, pressure and RIP measures become available, the potential for RIP to guide newborn resuscitation should be investigated.

Essentials to Remember

- RIP is a non-invasive method of measuring absolute or relative changes in thoracic volume.
- RIP is an accurate method of measuring breathing patterns and tidal volume, without the limitations associated with measurements at the airway opening.

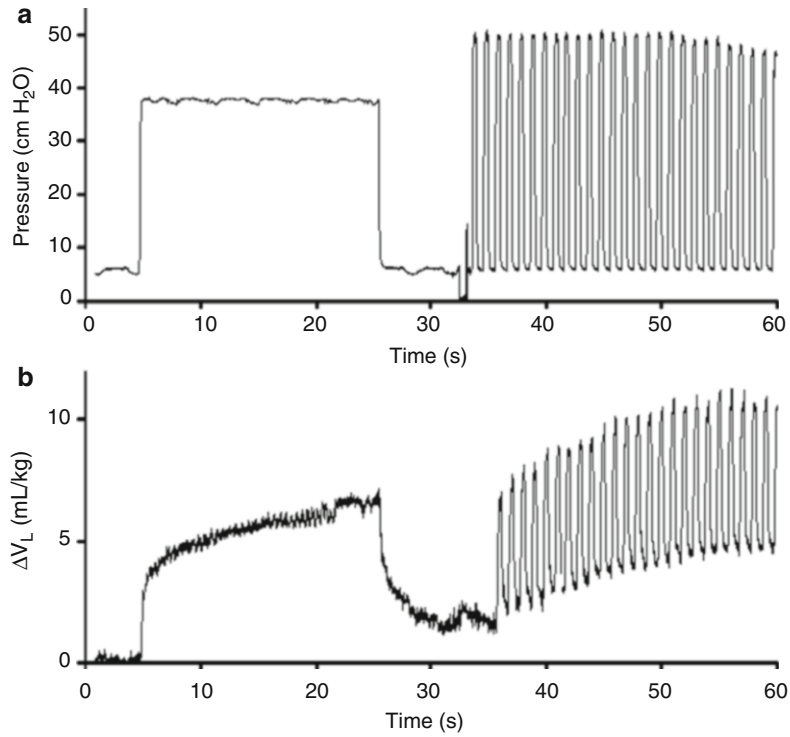

Fig. 14.8 Change in airway pressure (**a**) and lung volume (calibrated RIP, mL/kg; **b**) during a sustained inflation applied at birth, followed by positive pressure ventilation, in a preterm lamb

- More recently, RIP has shown promise as a reliable method of determining ΔEELV in the mechanically ventilated patient.
- At present, RIP remains an important tool for respiratory research at the bedside in ICU.
- In the future, with development of commercially available RIP units that overcome some of the inherent limitations present in current systems, RIP has the potential to be a valuable monitoring tool in paediatric and neonatal intensive care.

Educational Aims

This chapter aims to give an understanding of:

- The plethora of information on the heterogeneity of lung disease, the response to recruitment and the distribution of aeration that has been gained by computed tomography
- The value of other imaging techniques, including magnetic resonance imaging and positron emission tomography, in the study of the diseased lung
- The limitations of these imaging techniques in ventilated infants and children

14.2 Lung Imaging Methods

Peter A. Dargaville

14.2.1 Computed Tomography

The purpose of this section is to detail the advances in understanding of the diseased lung and its response to ventilation that have been made with the assistance of computed tomography. The use of CT imaging as a diagnostic tool in the ventilated infant and child is not discussed.

14.2.1.1 What Have We Learned from Computed Tomography of the Lung?

Since the earliest reports of the appearances of the lung in a ventilated subject using axial CT imaging (Brismar et al. 1985), a considerable body of knowledge has accumulated regarding the abnormalities of inflation and aeration in the diseased lung. Valuable insights have been gained both from experimental studies in animal models of lung disease and from ventilated humans, most of whom have been adults with acute respiratory distress syndrome (ARDS) (Gattinoni et al. 2001). In view of the radiation hazard, CT imaging specifically for delineation of patterns of aeration has not been performed in any systematic way in ventilated neonates, infants or children, but much of the data obtained in adult humans has direct relevance to even the smallest ventilated subject. The key observations made using CT imaging of the diseased lung are summarised in Table 14.1 and discussed further below.

Table 14.1 Information derived from computed tomography of the diseased lung

Inhomogeneity of lung expansion even with a relatively diffuse disease on plain X-ray
Effect of superimposed pressure on the dependent regions of the diseased lung
Presence of aeration "compartments" – non-aerated, poorly aerated, normally aerated and hyperinflated – in the diseased lung
Changes in lung aeration and recruitment (reduction in non-aerated lung) during ventilatory manoeuvres
Estimation of the potential for recruitment
Coincidence of recruitment and hyperinflation during tidal ventilation

A seminal observation from axial CT imaging in ARDS was that, in the face of relatively diffuse opacification on plain X-ray, lung densities are inhomogeneously distributed on axial CT slices (Fig. 14.9) (Gattinoni et al. 1986, 2001). It is now clear that ARDS is a patchy disease which includes areas of opacification and consolidation interspersed with regions in which relatively normal lung architecture and aeration remain. It is presumed that ARDS in infancy and childhood, as well as a number of neonatal lung diseases (including meconium aspiration syndrome), are similar morphologically. This has implications for the type of ventilation strategy to be used and its potential effectiveness, particularly if there are large areas of consolidation resistant to reinflation that are in juxtaposition with areas of relatively unaffected lung prone to hyperinflation.

Several descriptions of the morphological pattern of CT densities exist in ventilated patients with ARDS. The densities have been classed as diffuse, lobar or patchy (Puybasset et al. 2000), with the diffuse pattern being associated with a greater response to recruitment (Constantin et al. 2010). The pattern of lung densities has also been recognised to differ based on whether the lung disease is pulmonary or non-pulmonary in origin (Pelosi et al. 2003). In the latter case, the major impairment of compliance involves the chest wall, including the diaphragm, which may be subjected to significant limitation of movement in cases of abdominal sepsis or trauma (Pelosi et al. 2003). Not surprisingly, supra-diaphragmatic lung regions are most prone to atelectasis when there is diaphragmatic splinting of this type. Examples in childhood are a preterm infant with necrotising enterocolitis or a child with acute pancreatitis, but again no systematic CT imaging studies have been performed.

CT imaging in ARDS has also revealed that the inhomogeneous distribution of lung densities is, in part, gravity-related. The potential for superimposed pressure to cause compression atelectasis of dependent lung regions is now understood (Pelosi et al. 1994), as is the heightening of this effect in the diseased lung where the gas to tissue ratio is decreased throughout the

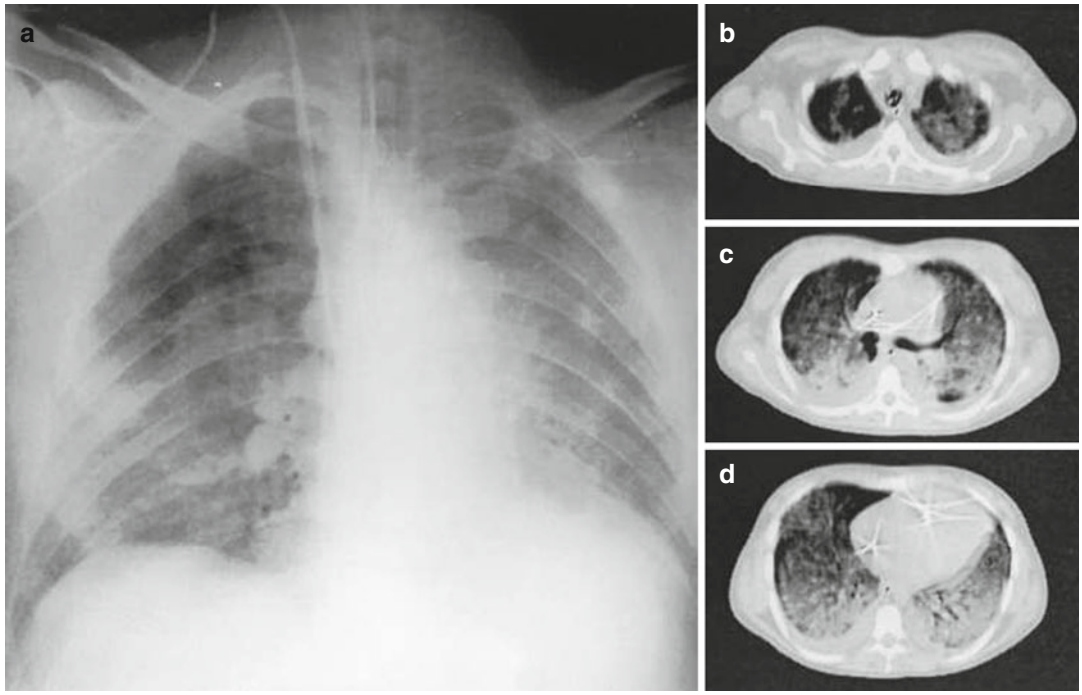

Fig. 14.9 Inhomogeneity of lung densities in acute respiratory distress syndrome. Anteroposterior chest X-ray (panel **a**) and axial CT scans at the level of the apex (**b**), hilum (**c**) and base (**d**) in a ventilated adult with acute respiratory distress syndrome from sepsis. Images were taken at a PEEP of 5 cm H_2O. The chest X-ray shows relatively diffuse opacification, sparing the right upper lung. The CT scans show inhomogeneous disease in both the craniocaudal and sternovertebral gradients (Reproduced from Gattinoni et al. (2001) with permission of the American Thoracic Society. Copyright © American Thoracic Society)

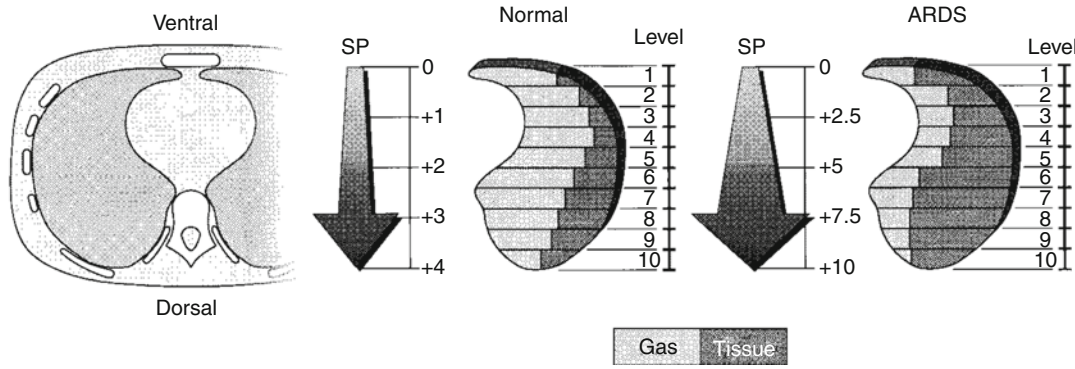

Fig. 14.10 The gradient of superimposed pressure. Increased mass of diseased lung (at *right*) causes in increased superimposed pressure, which, in turn, leads to a "gas squeezing" from the most dependent lung regions. Superimposed pressure is expressed as cm H_2O (Reproduced from Gattinoni et al. (2001) with permission of the American Thoracic Society. Copyright © American Thoracic Society)

lung (Fig. 14.10). CT imaging has shown that dependent atelectasis occurs in the normal lung under anaesthesia (Brismar et al. 1985) and can be identified in the full-term newborn with panalveolar disease (Fig. 14.11). Lung regions affected by dependent atelectasis are potentially recruitable with ventilatory manoeuvres, and this form of atelectasis can be counteracted by the use of positive end-expiratory pressure (PEEP) (Gattinoni et al. 1993). For overcoming the effects of superimposed pressure in the most dependent regions, theoretical considerations

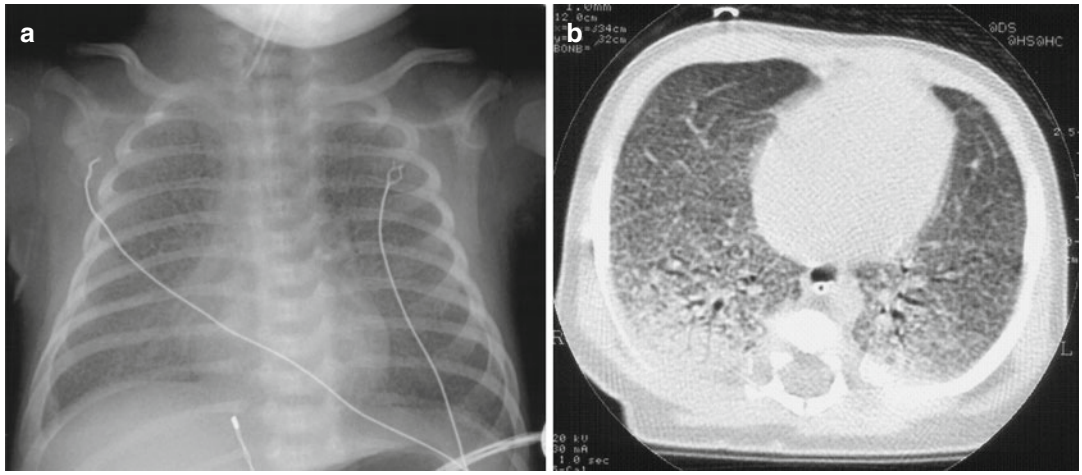

Fig. 14.11 Inhomogeneity in the ventral-dorsal axis revealed by CT scanning. Anteroposterior chest X-ray (panel **a**) and single-slice CT scan (panel **b**) from a 3-week-old ventilated infant with surfactant protein B deficiency. The chest X-ray shows diffuse reticulogranular opacification, reflecting the pan-alveolar nature of the disease. The CT shows the inhomogeneity of lung expansion in the anteroposterior axis, with dependent atelectasis largely attributable to superimposed pressure

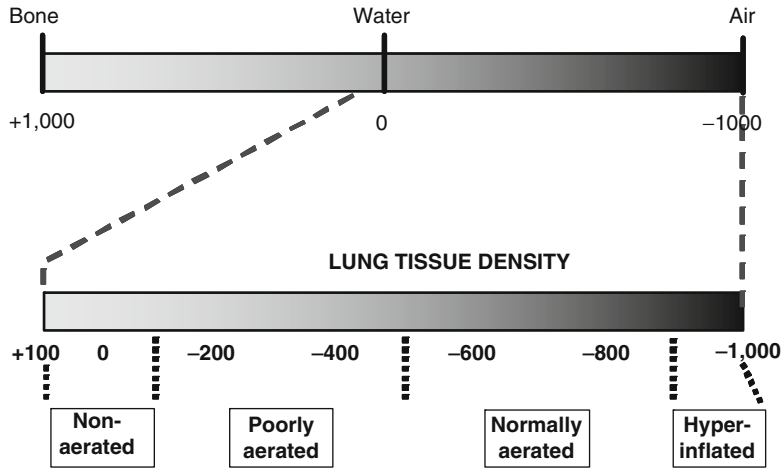

Fig. 14.12 The Hounsfield unit scale. The complete span of values from bone (+1,000) through water (0) to air (−1,000) is shown at top, and below, the range of values found in the normal and diseased lung. The lung parenchyma in a CT slice can be identified on the basis of Hounsfield scores as being non-aerated (+100 to −100), poorly aerated (−100 to −500), normally aerated (−500 to −900) or hyperinflated (−900 to −1,000)

would suggest that a PEEP level (in cm H_2O) equivalent to the anteroposterior diameter of the chest (in cm) is required. This estimate assumes a highly diseased lung with a gas to tissue ratio close to zero (Hickling 2001).

14.2.1.2 Measurements of CT Densities

CT imaging has allowed not only delineation of the morphological pattern of pulmonary densities but also a quantitative analysis of lung aeration and its alteration during ventilatory manoeuvres. The value of CT in this regard is the use of the Hounsfield unit (HU) scale (Fig. 14.12), which allows a gas to tissue ratio and gas volume to be derived for each voxel (CT volume unit) within an axial slice and also allows the lung to be separated into aeration "compartments" (Fig. 14.12). An aeration compartment is the cumulative sum of all lung units

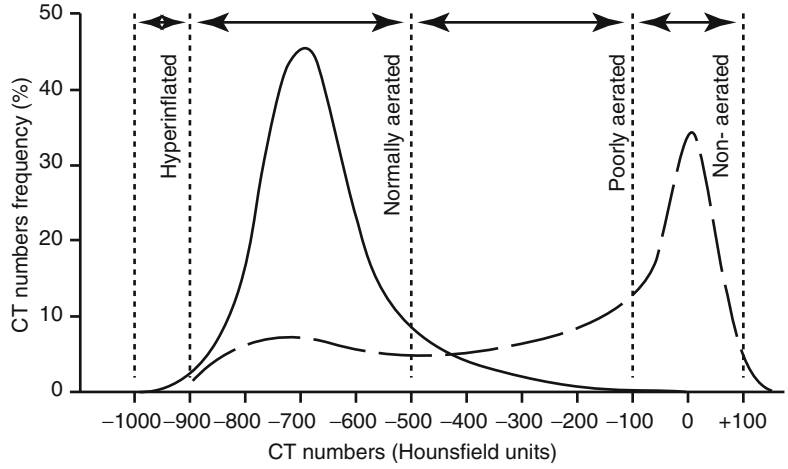

Fig. 14.13 CT histograms. Representative CT histograms from the normal lung (*solid line*) and a ventilated patient with acute respiratory distress syndrome (ARDS) (*dashed line*). Lung compartments, as defined by CT numbers, are indicated by the *dotted lines*. Note the predominance of non-aerated lung in the CT histogram in ARDS (Redrawn from Gattinoni et al. (2001) with permission of the American Thoracic Society. Copyright © American Thoracic Society)

in the CT slice having Hounsfield scores within a predefined range: non-aerated (−100 to +100 HU), poorly aerated (−100 to −500 HU), normally aerated (−500 to −900 HU) and hyperinflated (−900 to −1,000) (Gattinoni et al. 2001; Vieira et al. 1998). This information can be represented graphically in a CT histogram (Fig. 14.13), allowing the differences in aeration compartments to be highlighted in a normal and diseased lung.

Quantitative CT scanning has been used to measure changes in aeration compartments with ventilatory manoeuvres (Vieira et al. 1998; Crotti et al. 2001; Pelosi et al. 2001a; Albaiceta et al. 2004; Gattinoni et al. 2006; Lu et al. 2006; Pellicano et al. 2009). From these, much information has been gained about the nature of, and potential for, lung recruitment (Crotti et al. 2001; Pelosi et al. 2001b; Caironi et al. 2010), and the distribution of opening and closing pressures of lung units have been plotted (Crotti et al. 2001; Pelosi et al. 2001b). The impact of changes in ventilatory strategy has been demonstrated, including both the resolution of atelectasis at higher PEEP levels (Fig. 14.14) and the potential for overdistension (Vieira et al. 1998). This information has aided considerably in the understanding of application of ventilation to the diseased lung.

14.2.1.3 Limitations of CT Scanning

CT scanning has not been used in ventilated neonatal and paediatric subjects solely for the purpose of evaluating lung aeration and recruitment potential. This is chiefly because of concerns regarding radiation exposure (Mayo et al. 2003), although, with the advent of low-dose thin-section CT, the radiation dose may be 5–10 % of that with conventional CT imaging. Other limitations are lack of availability of CT scanning time and the difficulties and risks of transfer of ventilated neonatal and paediatric subjects to the CT scanning suite. For these reasons, it is unlikely that CT imaging will become widely used as a tool for evaluating regional lung inflation in this group. As discussed elsewhere in this text, there is potential for electrical impedance tomography to give similar information at the bedside of a ventilated subject, and experience with this form of imaging is growing (Frerichs et al. 2001a).

14.2.2 Magnetic Resonance Imaging

The use of magnetic resonance (MR) imaging of the lung parenchyma is essentially limited to quantification of lung water content and its spa-

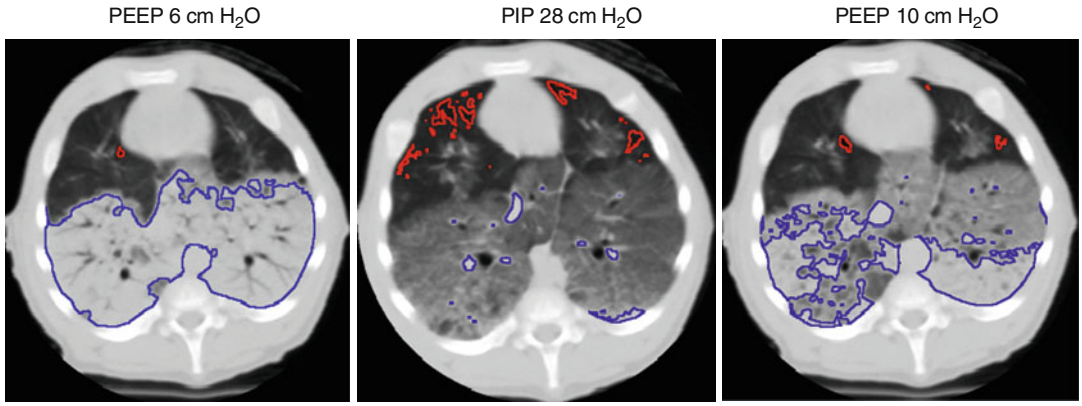

Fig. 14.14 Extremes of regional aeration during mechanical ventilation. Supra-diaphragmatic axial CT images in a 5 kg piglet with lung injury after repeated saline lavage. Areas of non-aerated lung (+100 to −100 HU) are traced in blue, and areas of hyperinflation (−900 to −1,000 HU) in red. At a PEEP of 6 cm H_2O, 53 % of the voxels are non-aerated, and only 0.15 % are hyperinflated. After a tidal inflation to a PIP of 28 cm H_2O, very little non-aerated lung remains (2 %), but there is demonstrably more hyperinflation (2.5 % of all voxels). Ventilation with a PEEP of 10 cm H_2O results in considerable improvement in end-expiratory collapse (22 % non-aerated), with minimal effect on hyperinflation (0.43 %)

tial distribution, using proton density-weighted images. Given the relative lack of fat and other hydrogen-bound complexes in the lung, there is a direct relationship between proton density and lung water content. Studies in experimental animals (Schmidt et al. 1986; Viard et al. 2008), as well as human adults (Mayo et al. 1995) and preterm infants (Adams et al. 2002), have confirmed that MR imaging can quantify the water content of the lung and indicate its distribution. A measurable increase in water content has been demonstrated in animals with experimental pulmonary oedema (Schmidt et al. 1986). Gravity-related maldistribution of lung water, with higher water content in the dependent regions, has been observed on MR imaging (Adams et al. 2002). Clearance of lung liquid after birth has been measured in preterm lambs using the technique (Viard et al. 2008).

A single report from a neonatal unit with an onsite MR imaging suite has provided information on the lung water content and distribution in the term and preterm newborn (Adams et al. 2002). The lungs of preterm infants showed considerably greater water content than their term counterparts and a more obvious sternovertebral gradient in water distribution (Fig. 14.15). Rapid redistribution of the density gradient occurred after turning prone, and lung water appeared to be more uniform in prone position than when supine (Adams et al. 2002).

Another application of MR imaging, not previously used in ventilated infants or children, is the use of hyperpolarised helium (^{3}He) as a means both of tracking distribution of ventilation (Rudolph et al. 2009) and, intriguingly, of measuring intrapulmonary oxygen concentration (Eberle et al. 1999). Access to high-grade ^{3}He gas and the gas delivery device required to control its administration are limiting factors to the wider application of this technique.

The limited availability of MR facilities, along with the need for non-ferrous ventilators and monitoring equipment, means that MR imaging is unlikely to become more widely used in the future for evaluation of either lung water content or ventilation distribution in neonatal and paediatric subjects on ventilatory support.

14.2.3 Positron Emission Tomography

Positron emission tomography (PET) is a three-dimensional functional imaging technique often combined with CT, which is based around detection of gamma radiation from a positron-emitting radionuclide. In the clinical setting, PET

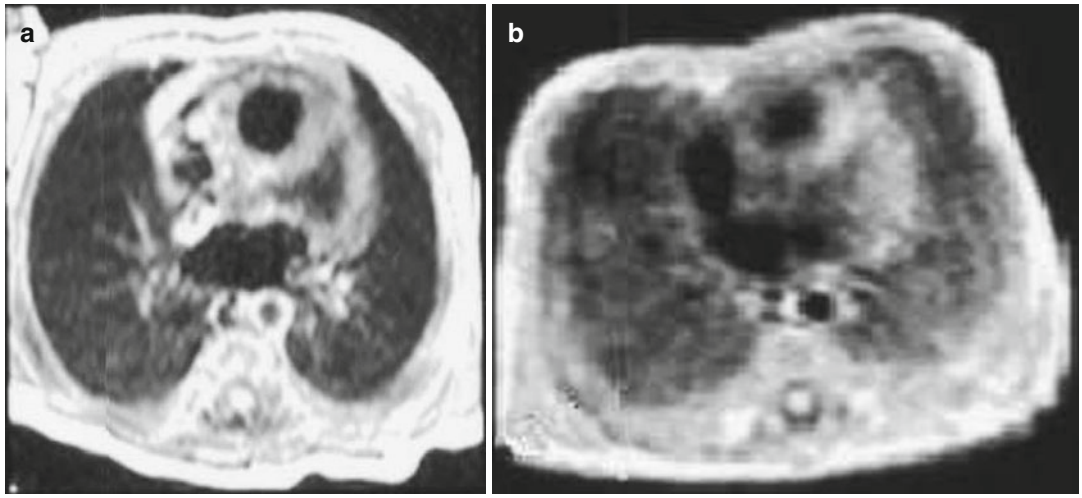

Fig. 14.15 Magnetic resonance images of the term and preterm lung. Cross-sectional T1-weighted magnetic resonance images at the level of the left atrium in a healthy term infant (panel **a**) and 26-week gestation infants at day 4 of life (panel **b**). Signal intensity in the lung parenchyma is higher in the preterm infant, with a more obvious anteroposterior gradient of increasing signal intensity, representative of increased parenchymal water content in the dependent lung regions (Redrawn from Adams et al. (2002) with permission of the American Thoracic Society. Copyright © American Thoracic Society)

scanning is used quite extensively for diagnostic imaging of suspected pulmonary malignancy. In the research laboratory, PET techniques have been applied in experimental animals for the estimation of regional lung perfusion and water content (Schuster and Howard 1994; Richard et al. 2002) and for the evaluation of pulmonary inflammation and ventilator-induced lung injury (Kirpalani et al. 1997; Monkman et al. 2004; Costa et al. 2010). These latter studies used ^{18}fluorodeoxyglucose, a tracer that is taken up into neutrophils and thus preferentially localises in areas of inflammation, including in the lung parenchyma. In newborn piglets, a clear increase in tracer uptake by the lung has been noted after injurious ventilation compared to controls with normal lungs (Kirpalani et al. 1997). Increased tracer uptake was seen in ventilated sheep with endotoxaemia to be localised to regions that were both aerated and perfused (Costa et al. 2010), suggesting that factors beyond gas distribution alone contribute to regional neutrophilic inflammation during lung injury with associated endotoxaemia.

A single investigative group has examined the possibility that PET scanning could discern differences in lung inflammation in preterm infants with and without exposure to inflammation prenatally (Andersen et al. 2003). No clear differences in ^{18}FDG uptake were observed in preterm infants with a history of maternal chorioamnionitis compared with those with no antenatal inflammation. Several infants with no apparent systemic inflammatory response had very high tracer uptake in the lung on PET scanning (Andersen et al. 2003). This study did not point to a potential role for PET scanning in the investigation of lung inflammation in the ventilated preterm infant, and no further studies have been forthcoming.

Essentials to Remember

- CT imaging of the diseased lung has revealed the heterogeneity of parenchymal densities, related both to random distributional effects and to gravity-related compressive forces acting on dependent regions.
- CT imaging in ventilated adults with acute respiratory distress syndrome can map the distribution of opening pressures and quantify the potential for recruitment in response to sustained airway pressure.

- MR imaging and PET scanning have contributed to the understanding of lung water content and distribution of aeration, but are not currently used in the clinical setting for these applications.
- The limited availability of these imaging techniques, coupled with technical difficulties peculiar to each, precludes a recommendation for their use in the management of ventilated infants and children with lung disease.

14.3 Bedside Lung Imaging Methods (Electrical Impedance Tomography)

Inéz Frerichs

Educational Aims

- To understand the measuring principle of EIT
- To learn how EIT is able to track changes in regional lung volumes and tidal volume distribution as well as to determine regional dynamic phenomena in lung ventilation
- To identify the potential benefit of functional EIT lung imaging in monitoring of ventilated neonatal and paediatric patients
- To identify the present limitations and drawbacks of EIT

14.3.1 Introduction

The use of established radiological imaging methods in respiratory monitoring of mechanically ventilated infants is limited especially because of the imposed radiation load or the necessity of patient transport to the examination site. Ventilated patients would benefit from new monitoring approaches providing instantaneous assessment of regional lung function at the bedside and enabling more rapid adjustment of ventilator settings. The non-invasive and radiation-free method of electrical impedance tomography (EIT) has recently been proposed as a possible future monitoring tool in this indication. EIT allows the assessment of regional lung ventilation and of changes in regional lung volumes based on the measurement of electrical properties of the lung tissue. EIT has no known hazards and can be applied at the bedside. However, EIT has not been used routinely in a clinical setting, thus, its usefulness still has to be proved. Several small clinical studies in neonatal and paediatric patients indicate the potential of EIT monitoring. To establish the method as a routine medical examination tool, further development of the EIT hardware and software is necessary. Definition of the most adequate EIT examination procedures providing measures suitable for clinical decision-making and optimising the ventilator therapy is the other prerequisite.

14.3.2 Technique

14.3.2.1 Electrical Bioimpedance

The idea of imaging the human body by electrical current is not new. It is based on the fact that the tissue electrical properties are not uniform and vary among different organs (Geddes and Baker 1967). Biological tissues can conduct electrical current; however, their opposition to the transmission of current is not the same.

In general terms, any opposition of a medium to transmission of a time-varying signal is called impedance. If this medium is a biological tissue, then we speak of bioimpedance. If the time-varying signal used to probe the biological tissue is alternating electrical current, then the term electrical bioimpedance is used. The measurement of electrical bioimpedance is already being utilised by a few medical technologies (Table 14.2). In electrical impedance tomography (EIT), images of the distribution of electrical bioimpedance within the body are generated.

Table 14.2 Medical examination techniques based on the measurement of electrical bioimpedance

Method	Main information retrieved
Bioimpedance analysis	Body composition
Impedance cardiography	Cardiac output
Impedance pneumography	Respiratory rate
Impedance tomography	Body imaging

The first attempts to produce electrical bioimpedance images of the body originate already from the late 1970s of the last century. They aimed at generating anterior to posterior chest images, similar to chest radiography (Henderson and Webster 1978). The first EIT system producing cross-sectional, i.e. tomographic images of the human body was developed by David C. Barber and Brian H. Brown in the early 1980s of the last century (Barber and Brown 1984).

14.3.2.2 EIT Setup

EIT uses a set of measurement electrodes which are attached on the surface of the studied body section. If an EIT examination is performed on the chest, then the electrodes are placed on the chest circumference usually in one transverse plane (Fig. 14.16). The electrodes either are integrated in an electrode band or are individually attached on the thorax wall. In the latter case, conventional self-adhesive ECG electrodes may be used. The use of X-ray translucent electrodes is also possible. The electrodes are connected with the EIT device by leads.

Most of the currently used EIT systems use an array of 16 electrodes. This number of electrodes is a good compromise securing sufficient image resolution and equidistant placement of electrodes without the risk of undesirable accidental electrode contact. Eight- and thirty-two-electrode EIT systems have also been developed; however, the loss in spatial resolution or the necessity of placing a large number of electrodes on the chest makes these systems less adequate.

14.3.2.3 EIT Data Acquisition

During an EIT examination, minute alternating electrical currents are injected into the body. These currents have an amplitude of only a few mA and a frequency in the range of approximately 10 kHz–1 MHz. The currents are applied between adjacent pairs of electrodes in most of the EIT systems. The current-carrying electrode pairs are cyclically activated, and the current injection rotates around the body. During each application of electrical current, the resulting potential differences are measured between all other passive electrode pairs. The voltage distribution developed on the surface of the chest is determined by the internal distribution of electrical resistances within the chest and its shape. Also in the case of voltage measurement, adjacent electrodes are preferentially used. With the described 16-electrode arrangement and pattern of rotating current application and voltage measurement, a total of 208 voltage values are acquired during each scan cycle. The maximum EIT scan rate is rather high. With up to 50–60 scans/s, it is much higher than in other, classical radiological tomographic methods, like computed tomography or magnetic resonance imaging.

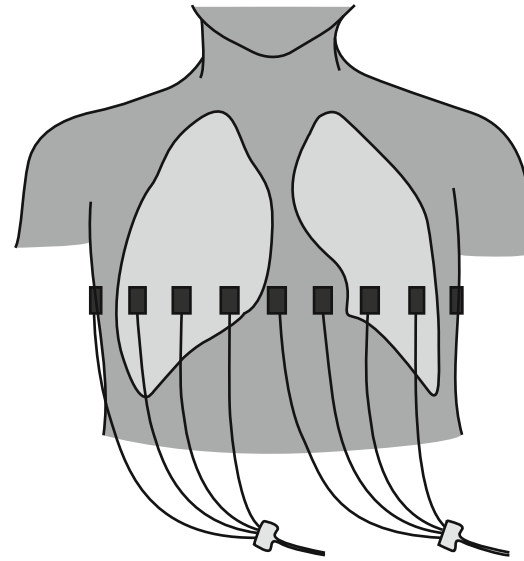

Fig. 14.16 Measuring principle of EIT. An array of surface electrodes is attached on the chest circumference in one transverse plane and connected via leads with the EIT device. Very small alternating electrical currents are consecutively applied through all adjacent pairs of electrodes. The resulting potential differences are measured at all passive electrode pairs during each current application. The process of current applications and acquisitions of potential differences rotates around the chest at high rates

14.3.2.4 EIT Image Reconstruction

The set of electrical voltages acquired at the chest surface as a result of electrical current application during each scan cycle is used to calculate the distribution of electrical impedance within the thorax. The calculated impedance values are then converted to a two-dimensional, cross-sectional EIT scan in an either grey or colour scale. This process of generation of impedance distribution images from the measured potential differences and known excitation currents is called image reconstruction (Barber 1990; Morucci and Marsili 1996).

The generation of EIT scans is not easy. This is first of all related to the fact that the human body is a three-dimensional object. Electrical currents applied through the electrodes at the boundary of the chest are not confined to the two-dimensional transverse plane, defined by the electrode array. The currents also flow into more distant regions, and their pathways are not known. This means that EIT scans always reflect not only the impedance distribution in the studied plane but are also affected by tissues lying outside of the measurement plane, although with lower sensitivity. Another point is that the currents tend to penetrate less into the deeper chest regions. Therefore, the spatial resolution also tends to be poorer in the centre than at the chest periphery.

In general, there exist three major ways how EIT scans can be generated (Boone et al. 1997). The first approach aims at depicting the distribution of absolute values of electrical impedance within the chest. Although such images have already been obtained in vivo, their quality was rather poor. This is mainly because these images are very sensitive to EIT data collection errors and require the knowledge of the shape of the body. The same limitations also apply to the second approach, which tries to differentiate the tissues based on their varying response to electrical currents of different frequencies. The most frequently used approach is the third one, in which changes or differences in electrical impedance are determined and converted to EIT scans. The advantages of this approach are that errors tend to cancel and the uncertainties about the body shape do not affect the image quality. The calculated impedance changes are often normalised by relating them to a reference state of impedance. This is, for instance, done when the so-called weighted backprojection (Barber 1990) is used, which has been the most often used method of EIT image reconstruction in in vivo EIT imaging so far. All EIT scans shown in the figures in this chapter have been generated using this type of image reconstruction.

The weighted backprojection algorithm is a rather old approach to image reconstruction known to be associated with several assumptions which are not met during measurements in humans. Nevertheless, it has been successfully applied in multiple clinical studies. Several other EIT image reconstruction algorithms have been developed over the past 20 years; however, their performance has mostly been tested only under in vitro conditions. EIT image reconstruction is one of the most active fields in EIT research. Only recently, an initiative of a large and representative group of experts has been formed to develop a unified reconstruction algorithm for lung EIT imaging which should secure the highest possible and uniform spatial resolution, accuracy and sensitivity (Adler et al. 2009).

14.3.3 Image Interpretation and Qualitative Analysis

An EIT chest examination results in a series of EIT scans acquired during a selected period of time (Fig. 14.17). In ventilated patients, these scans usually cover a period of multiple breaths, a ventilation manoeuvre (for instance, a pressure-volume manoeuvre, suctioning) or another intervention (change in ventilator settings or mode).

Such series of individual EIT scans can be displayed directly online during the data acquisition or offline after the completion of the examination. Thanks to the high EIT scan rates, they result in a video sequence of the instantaneous distributions of electrical impedance in the chest. Such videos are dominated by the large impedance changes associated with the variation in regional lung volume; the much smaller changes in the cardiac region are often also discernible.

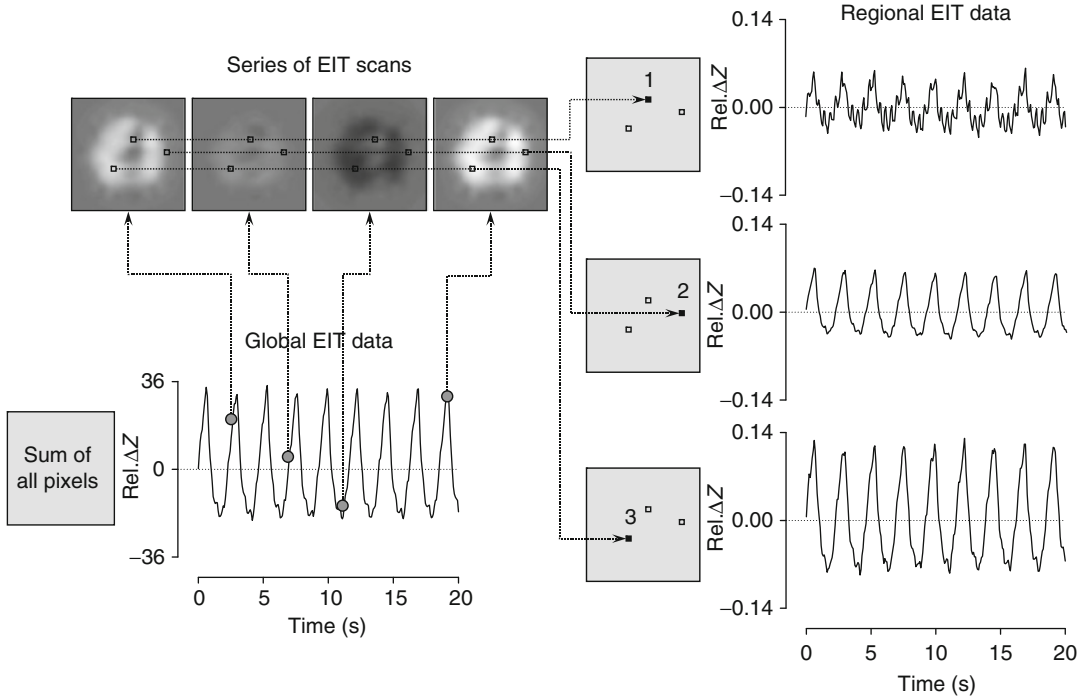

Fig. 14.17 Chest EIT scans and regional EIT tracings. During an EIT examination, a series of EIT scans is acquired showing the instantaneous distribution of electrical impedance changes in the chest cross-section relative to a reference state (*top left*). In this example, the reference impedance distribution corresponded to the average impedance distribution during a 20-s long phase of mechanical ventilation. Thus, the EIT scans show higher regional impedance values at higher regional lung volumes (*light tones*), lower values at lower volumes (*dark tones*) or minimum changes when the regional lung volumes were close to the reference volumes. The tracing of global EIT data (*bottom left*) was generated by summing up all 912 image pixel values of relative impedance change (rel.$\mathbf{\Delta}Z$) in each scan of the acquired series and plotting them as a function of time. An increase in impedance values occurs during inspiration, a fall in impedance is observed during expiration. The light grey circles and the dotted arrows indicate at which moment of the respiratory cycle; the four EIT scans were obtained. The tracings of regional EIT data (*right*) originate from three image pixels shown as small squares in the EIT scans. The *top* tracing is a plot of a time series of local relative impedance change obtained in pixel 1 which was located in an anterior region of the chest. Thus, the signal contains impedance changes related to ventilation superimposed on which are the more frequent changes synchronous with the heart rate. The *middle* tracing originates from the pixel 2 located at the edge of the left lung region showing predominantly the ventilation-related impedance changes. The *bottom* tracing was obtained in the pixel 3 in the right lung region and shows the highest ventilation-related changes in impedance with time. (The EIT data presented in this figure originate from an EIT examination of an 8-week-old infant with a body weight of 4,585 g and a length of 56 cm. The infant suffered from posthaemorrhagic hydrocephalus and was studied in the operating room prior to surgery during continuous positive pressure ventilation with a tidal volume of 10 mL/kg body weight and positive end-expiratory pressure of 4 cm H_2O. The respiratory rate was 26 breaths/min, the inspiration/expiration ratio was 1/1 and the fraction of inspired O_2 23 %)

The even smaller cyclic EIT signal variation caused by lung perfusion is usually masked by the large impedance changes during ventilation. Thus, lung perfusion only becomes visible in such video sequences when the lung air content does not change, e.g. during apnoea. The series of individual EIT scans are usually considered only the first step in further evaluation.

EIT can track rapid regional changes in electrical impedance in the chest cross-section resulting from the physiological processes like ventilation, heart action or lung perfusion. Figure 14.17 illustrates this capability of EIT by showing the regional tracings of EIT data in three image pixels. These tracings reveal the typical ventilation-related variation of the EIT signal as well as the

heart beat synchronous variation detectable especially in the heart region. The excellent time resolution of EIT with high scan rates allows even more frequent events to be tracked, like the very small and rapid air volume oscillations during high-frequency oscillation ventilation.

Thus, the regional pixel tracings of EIT data contain valuable compressed information on different aspects of the lung function which can be addressed and evaluated using various functional evaluation approaches. Functional EIT imaging allows the generation of the so-called functional EIT scans from the series of individual EIT scans which provide condensed and separate information on one selected aspect of the lung function, e.g. the spatial distribution of lung volume changes or tidal volumes, as will be described in the next text section. A series of individual EIT scans containing hundreds or even thousands of scans may serve as a basis for generation of several types of functional EIT scans. For instance, the functional EIT scan in Fig. 14.18 was generated from the 20-s series of 500 EIT scans shown in Fig. 14.17 and characterises the ventilation distribution in the chest cross section during this EIT examination.

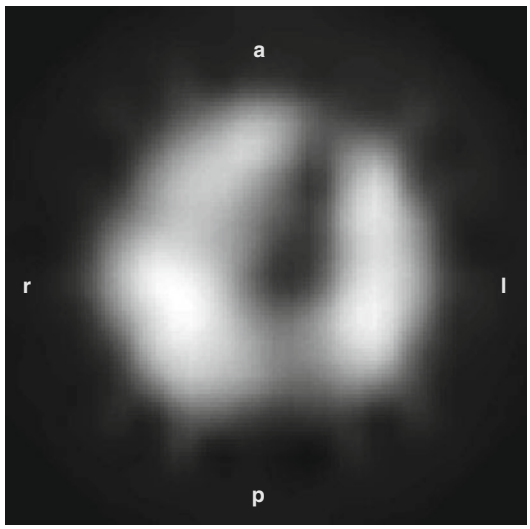

Fig. 14.18 Functional EIT scan showing the distribution of tidal volume in the chest cross-section. This scan was generated from the same EIT examination presented in Fig. 14.17 by calculating the average regional tidal, i.e. inspiratory to expiratory difference in electrical impedance in each image pixel during 20 s of mechanical ventilation. The spatial orientation of the scan is indicated (*a* anterior, *p* posterior, *r* right, *l* left)

14.3.4 Tracking Lung Volumes and Tidal Volume Distribution

14.3.4.1 Changes in Regional Lung Volumes

The ability of EIT to track regional lung volume changes has been validated by several established imaging modalities (computed tomography, positron emission tomography, single-photon emission computed tomography, ventilation scintigraphy) (Frerichs et al. 2002; Hinz et al. 2003b; Kunst et al. 1998; Richard et al. 2009; Serrano et al. 2002; Victorino et al. 2004; Wrigge et al. 2008) and other medical methods (spirometry, inert gas washout) (Hahn et al. 1995; Harris et al. 1987; Hinz et al. 2003a).

An increase in the lung air content leading to a rise in lung volume is accompanied by an increase in electrical impedance. Electrical impedance falls when lung volume decreases. These typical impedance changes occur regularly during the respiratory cycle both during spontaneous breathing or mechanical ventilation. In ventilated patients, additional lung volume changes may result from altered ventilator settings.

Changes in positive end-expiratory pressure (PEEP) influence the aeration of the lungs and, consequently, the impedance level, on which the cyclic ventilation-related variation of the EIT signal is superimposed (Erlandsson et al. 2006; Frerichs et al. 1999a, 2003a; Meier et al. 2008). The changes in aeration may be spatially inhomogeneous, and it is the advantage of EIT that it can track these aeration changes on a regional level. For instance, an increase in regional electrical impedance in the dependent lung regions after an increase in PEEP may indicate alveolar recruitment. Merely a small increase in impedance in the nondependent regions with a pronounced effect in other regions may hint at possible local overdistension.

Figure 14.19 illustrates the potential of EIT in tracking regional lung volumes in another exam-

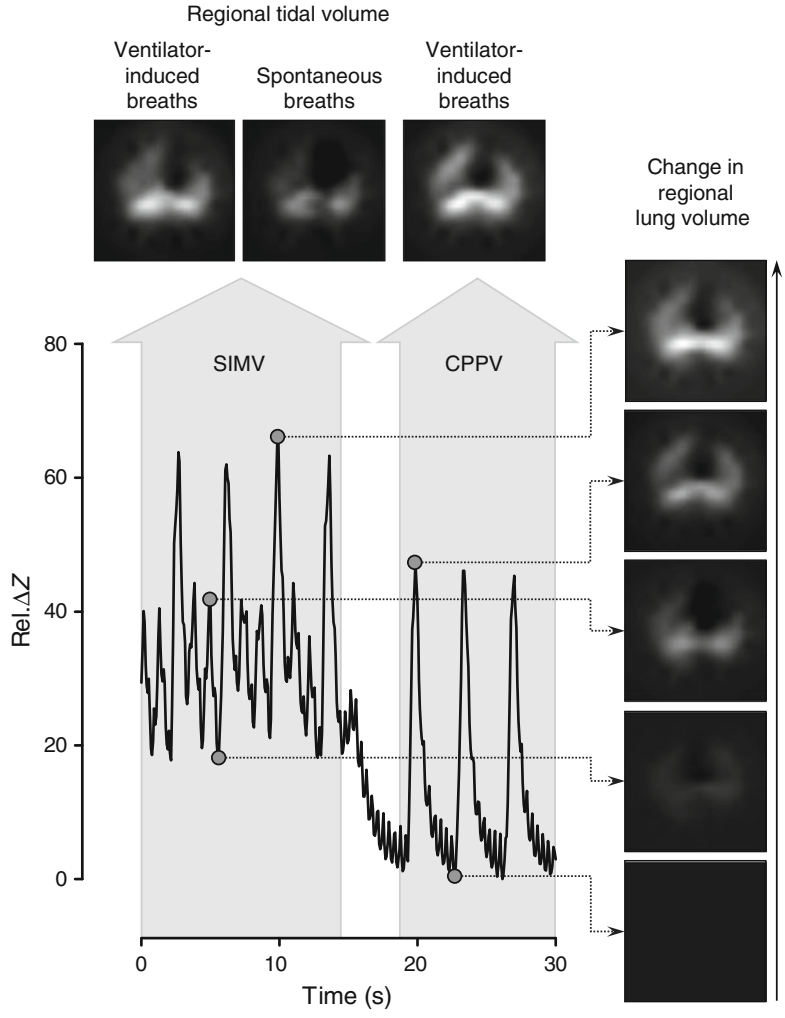

Fig. 14.19 EIT examination during weaning from mechanical ventilation. A 30-s tracing of global EIT data is shown, generated by summing up all 912 EIT image pixel values of relative impedance change (rel.**Δ***Z*) from a series of 750 EIT scans. The examination was performed in a 10-week-old preterm infant with a body weight of 2,500 g and a length of 44 cm. The data was acquired in a neonatal intensive care unit during postoperative weaning from mechanical ventilation after orchiopexy. The infant was ventilated in an assisted mode with synchronised intermittent mandatory ventilation (*SIMV*). The respiratory rate was 16 breaths/min, the inspiration/expiration ratio was 1/5.2, positive end-expiratory pressure 3 cm H_2O, peak inspiratory pressure 24 cm H_2O and the fraction of inspired O_2 21 %. During the initial phase of the examination, highlighted by the first light grey area, the EIT signal reflects the typical lung volume changes occurring in the lungs during SIMV: the four large deflections represent the larger ventilator-induced breaths, the smaller deflections in between originate from the smaller spontaneous tidal breaths. During the subsequent short apnoea, the impedance values fall to a new end-expiratory level due to loss in lung volume, followed by three-controlled ventilator-induced breaths during continuous positive pressure ventilation (*CPPV*), highlighted by the second *light grey area*. The small and rapid impedance signal fluctuations, discernible especially during the apnoeic and CPPV phases, are synchronous with the heart rate of 152 beats/min. The three images at the *top* of the figure are functional EIT scans showing the distribution of tidal volumes: the left two of these scans were generated from the SIMV phase and provide the distribution of both ventilator-induced and spontaneous breaths, and the right image shows the tidal volume distribution during CPPV. Of note is the more pronounced ventilation of anterior lung regions during fully controlled ventilation without spontaneous breathing activity. The five functional scans on the right show the changes in regional lung volume at different phases of the EIT examination compared with the lowest volume at end-expiration during CPPV

ple. This EIT examination was performed in a ventilated infant during weaning and shows the loss in lung volume after temporary cessation of spontaneous breathing activity during assisted ventilation. The lowest level of lung aeration was noted at end-expiration after the spontaneous breathing had ceased. Functional EIT scans can be generated which visualise the instantaneous level of aeration at different time points of the examination.

14.3.4.2 Tidal Volume Distribution

During tidal spontaneous or artificial ventilation, the highest values of electrical impedance occur at end-inspiration, the lowest at end-expiration. The differences between the regional peak and trough values of the EIT signal are representative of regional tidal volumes. If these regional differences between the maximum and minimum impedance values are calculated from one or more respiratory cycles in each image pixel, they may be converted in another type of a functional EIT scan showing the distribution of tidal volume in the chest cross-section.

The distribution of tidal volume is influenced by the type of ventilation (spontaneous vs. mechanical), body position and gravity and by the local mechanical properties of the lung tissue which may be nonhomogeneously altered by lung pathology. Figure 14.19 shows how the tidal volume distribution may vary even within a very short time interval. In the course of this EIT examination, which was already referred to in the above text, the studied infant was ventilated in an assisted mode of ventilation. Ventilation was accomplished by ventilator-induced breaths in combination with spontaneous breathing activity. The functional EIT scans of tidal volume distribution generated from this phase of the EIT examination show that the regional tidal volumes were smaller during the spontaneous than ventilator-induced breaths; nevertheless, their spatial distribution was similar. An interesting phenomenon is revealed when the distribution of the ventilator-induced tidal volumes is compared between this phase and the phase when the infant ceased to breathe spontaneously. A more pronounced distribution of the tidal volume to the nondependent anterior regions was found in the latter phase indicating that a spatial redistribution of tidal volume had occurred when the mechanical breaths were applied at a lower end-expiratory lung volume.

14.3.4.3 Combination of Functional EIT Information

It was explained in the above text that functional EIT scans of various types can be generated from the same EIT examination by application of various evaluation steps and procedures. Figure 14.19 provided an example in which functional EIT scans showing the tidal volume distribution and regional lung volume changes relative to the lowest end-expiratory volume were obtained from the same EIT data by different analysis. The interpretation of multiple functional EIT scans may offer a deeper insight into the regional lung function. Even more detailed understanding could be obtained if functional EIT information is extracted from examinations performed during predefined manoeuvres, for instance, during a PEEP trial (Frerichs et al. 2003a; Meier et al. 2008).

The high scan rates achievable during EIT examinations allow an assessment of rapid dynamic phenomena in the regional lung function. Therefore, not only the above-mentioned regional lung volume changes and tidal volumes can be measured but also the dynamics of regional lung filling and emptying described (Frerichs et al. 2001b). For instance, progressive filling of lung regions characterised by an increasing rate of impedance change may occur during tidal lung recruitment or degressive filling with a decreasing rate of impedance change may arise from overinflation (Hinz et al. 2007). A regional time delay in an increase in impedance during lung inflation (Wrigge et al. 2008) may be a sign of airway collapse with delayed opening of the affected lung units. Regional tracings of the EIT signal registered after a stepwise change in airway pressure may be used to calculate the distribution of regional time constants.

Since many of the physiological processes in the lungs like ventilation and cardiac action,

which contribute to the time variation of the EIT signal, are of cyclic origin, they can be separated by using frequency filtering procedures (Dunlop et al. 2006; Frerichs et al. 2001a, 2009). Independent analysis of these processes is then possible. For instance, the functional EIT scans of tidal volume distribution during ventilator-induced and spontaneous breaths during assisted ventilation shown in Fig. 14.19 could easily be generated because the ventilator and spontaneous breathing rates were not equal.

Thus, a variety of information on different aspects of regional lung function can be obtained from EIT examinations (Bodenstein et al. 2009; Brown 2003; Costa et al. 2009; Frerichs 2000). There exist two ways how this information can be used in clinical decision-making: (1) It can be visualised in form of functional EIT scans. This way of presentation is suitable if rapid information on the spatial distribution of a chosen relevant lung function measure is needed. (2) Alternatively, the relevant EIT lung function measure can be calculated in meaningful pulmonary regions of interest (Pulletz et al. 2008; Victorino et al. 2004; Zhao et al. 2009) and used in its numeric form, for instance, to follow regional changes in lung function over time. EIT data are then acquired during a longer monitoring interval or as a series of short but repetitive examinations. This approach may be applied, for example, to establish if a recruitment manoeuvre or a change in ventilator settings opened an atelectatic region with a non-transient effect on regional tidal volume.

14.3.5 Clinical Experience

Clinical experience with EIT use for lung imaging in neonatal and paediatric patients is scarce. Until 2009, less than 20 EIT studies have been conducted in this patient group, mostly in rather small numbers of patients. The number of experimental and clinical studies in adults is much higher. Many of these studies possess a high degree of relevance for EIT application in the neonatal/paediatric field.

EIT studies in neonates and infants have mostly been motivated by two goals. The first one was to utilise the full non-invasiveness and lack of radiation of this new examination method to study such phenomena in the lung function which were previously not accessible to other established medical modalities or not ethically justified. EIT enabled regional analysis of lung function in preterm infants or neonates. Even lung healthy babies could be examined by EIT during undisturbed spontaneous breathing. Since very little is known about the regional lung function in patients of this age group, EIT was able to provide valuable information on the ventilation distribution under a variety of conditions. For instance, the significant effects of body and head position and the influence of the respiratory pattern (e.g. respiratory rate, sighs) on the spatial distribution of ventilation were established (Frerichs et al. 2003b; Heinrich et al. 2006). Furthermore, the differences in regional ventilation between preterm and term neonates could be addressed (Riedel et al. 2009). The specific features of the neonatal ventilation distribution pattern have been studied and compared with adults (Dunlop et al. 2006; Schibler et al. 2009; Smallwood et al. 1999). A few studies have been performed in neonates with the aim of determining the effect of maturational changes on the lung electrical properties, showing that increased alveolisation is associated with higher electrical impedance of the lung tissue (Brown et al. 2002a, b).

The other studies were motivated by the awareness of the potential of EIT in monitoring ventilated infants. EIT was applied to determine the effects of changed ventilator settings or therapeutic procedures (surfactant administration, suctioning) on regional lung function. These studies were performed in neonatal and paediatric intensive care units and provided the first evidence that useful feedback information can be generated by EIT at the bedside. The studied infant patients were followed by EIT during spontaneous breathing and different modes of mechanical ventilation (e.g. non-invasive and invasive ventilation in fully controlled conventional and high-frequency oscillation modes or assisted ventilation). It has been demonstrated that the immediate effects of changing PEEP, peak inspiratory pressure, inspiration-to-expiration time ratio and fraction

of inspired O_2 on the spatial distribution of ventilation were discernible (Frerichs et al. 2001a). Long-term monitoring of several days duration was also successfully accomplished to study regional lung ventilation in a critically ill neonate before and after cardiac surgery (Frerichs et al. 1999b). It has also been shown that rapid, regionally heterogeneous derecruitment induced by suctioning can be detected by EIT in children suffering from ARDS (Wolf et al. 2007). Finally, regional end-expiratory lung volumes were determined by EIT in ventilated infants with respiratory failure due to a respiratory syncytial virus infection (Kneyber et al. 2009).

14.3.6 Limitations and Drawbacks

Although EIT certainly exhibits many features which make this medical technology interesting for monitoring regional lung function in neonatal and paediatric patients, it is too early to say whether it will be able to prove its applicability and value in a routine clinical setting. Table 14.3 summarises the pros and cons of EIT imaging from the today's point of view.

Table 14.3 Pros and cons of EIT lung imaging

Advantages	Disadvantages
Non-invasiveness, no exposure to radiation, no known hazard	Poor spatial resolution
Low price	Necessity of surface electrodes or electrode bands
Small size, portability, bedside application	Hardware and software not yet optimised for clinical routine
Generation of tomographic images of a new biological quality	Procedures and quantitative parameters for clinical decision-making not yet defined
Good temporal resolution (i.e. high scan rate)	Large clinical studies lacking
Continuous examination (i.e. monitoring)	
Functional imaging	

With a clear lack of other alternative medical modalities suitable for monitoring regional lung function in ventilated infants at the bedside EIT possesses many intriguing characteristics: It allows continuous measurement of regional lung volumes and tidal volume distribution as well as the assessment of other regional measures characterising the dynamics of lung behaviour during mechanical but also spontaneous breathing. To obtain this kind of information, no radiation exposure is necessary; there exist no known hazards. After the application of EIT electrodes on the chest, continuous EIT scanning can easily be performed and interrupted any time.

The disadvantages of EIT comprise first of all the relatively low spatial resolution of EIT scans. Although continuous technological development and use of more advanced image reconstruction procedures can be expected to improve the EIT image quality, image resolutions as known in conventional chest radiography, computed tomography and magnetic resonance imaging will never be possible (Seagar et al. 1987). However, it has to be pointed out that EIT is not intended to be recommended as a sole imaging method. A meaningful combination of patient examinations using conventional imaging modalities, providing excellent anatomical information, and EIT, providing functional information, should be aspired. The conventional methods will make intermittent information on lung morphology available; EIT will offer continuous monitoring of lung function.

The essential drawback of EIT at present is that it has hardly been applied in large clinical trials. The final proof of clinical relevance and efficacy is still lacking. Many of the intriguing data obtained by this method in ventilated neonates and infants were merely small observational studies, in part, simple case reports. This means that EIT must be applied in larger groups of patients with clearly defined goals and outcome measures. One of the most important objectives should be the definition of appropriate procedures for standardised EIT examination of patients. Such procedures should provide relevant EIT measures suitable for clinical decision-making and optimisation of ventilator therapy. Since EIT has the perspective of becoming a broadly used monitoring tool at the bedside, it will be operated by the medical personnel and not

only by a few specialists, as is the case today. Therefore, factors like practicability of application and user friendliness of EIT data acquisition and evaluation will also play an important role in the clinical implementation of this technology.

14.3.7 Perspectives

EIT has the potential of becoming a bedside monitoring tool for monitoring regional lung function in ventilated neonatal and paediatric patients. This perspective is based on (1) the clinical need for improved patient monitoring, (2) several positive characteristics of this technology which are superior to other existing imaging modalities and (3) promising findings of hitherto existing EIT studies. The present interest in EIT is mainly driven by the increasing knowledge of possible detrimental effects of mechanical ventilation. If EIT monitoring succeeds to be established in a clinical setting, then it may provide online feedback on regional lung function and its changes in response to modified ventilator settings and other therapeutic procedures. This may facilitate individually optimised mechanical ventilation and minimise the incidence of ventilator-induced lung injury.

Essentials to Remember

- EIT is a non-invasive, radiation-free bedside medical imaging modality.
- EIT generates cross-sectional images of distribution of electrical bioimpedance within the chest.
- EIT allows functional lung imaging, thanks to very high scan rates.
- Functional EIT is able to determine changes in regional lung volumes and tidal volume distribution as well as regional dynamic phenomena in lung ventilation.
- Ventilated patients may benefit from future EIT monitoring since an immediate feedback on regional lung function may facilitate rapid adjustment of ventilator settings.

References

Adams JA (1996) Respiratory inductive plethysmography. In: Stocks J, Sly PD, Tepper RS, Morgan WJ (eds) Infant respiratory function testing, 1st edn. Wiley-Liss, New York

Adams JA, Zabaleta IA (1993a) Tidal volume measurements in newborns using respiratory inductive plethysmography. Am Rev Respir Dis 148:585–588

Adams JA, Zabaleta IA (1993b) Measurement of breath amplitudes: comparison of three noninvasive respiratory monitors to integrated pneumotachograph. Pediatr Pulmonol 16:254–258

Adams JA, Zabaleta IA (1994) Comparison of supine and prone noninvasive measurements of breathing patterns in full term newborns. Pediatr Pulmonol 18:8–12

Adams EW, Counsell SJ, Hajnal JV, Cox PN, Kennea NL, Thornton AS, Bryan AC, Edwards AD (2002) Magnetic resonance imaging of lung water content and distribution in term and preterm infants. Am J Respir Crit Care Med 166:397–402

Adler A, Arnold JH, Bayford R, Borsic A, Brown B, Dixon P, Faes TJ, Frerichs I, Gagnon H, Garber Y, Grychtol B, Hahn G, Lionheart WR, Malik A, Patterson RP, Stocks J, Tizzard A, Weiler N, Wolf GK (2009) GREIT: a unified approach to 2D linear EIT reconstruction of lung images. Physiol Meas 30:S35–S55

Albaiceta GM, Piacentini E, Villagra A, Lopez-Aguilar J, Taboada F, Blanch L (2003) Application of continuous positive airway pressure to trace static pressure-volume curves of the respiratory system. Crit Care Med 31:2514–2519

Albaiceta GM, Taboada F, Parra D, Luyando LH, Calvo J, Menendez R, Otero J (2004) Tomographic study of the inflection points of the pressure-volume curve in acute lung injury. Am J Respir Crit Care Med 170:1066–1072

Andersen C, Kent A, Schmidt B, Nahmias C, deSa D, Bourgeois J, Xing Z, Kirpalani H (2003) Pulmonary fluorodeoxyglucose uptake in infants of very low birth weight with and without intrauterine inflammation. J Pediatr 143:470–476

Barber DC (1990) Quantification in impedance imaging. Clin Phys Physiol Meas 11(Suppl A):45–56

Barber D, Brown B (1984) Applied potential tomography. J Phys E Sci Instrum 17:723–733

Bar-Yishay E, Putilov A, Einav S (2003) Automated, real-time calibration of the respiratory inductance plethysmograph and its application in newborn infants. Physiol Meas 24:149–163

Bhatia R, Owen LS, Davis PG, Tingay DG (2010) Stability of end-expiratory lung volume signal in three different respiratory inductive plethysmographs. J Paediatr Child Health 46 (Suppl 1):8 [abstract]

Bodenstein M, David M, Markstaller K (2009) Principles of electrical impedance tomography and its clinical application. Crit Care Med 37:713–724

Boone K, Barber D, Brown B (1997) Imaging with electricity: report of the European concerted action on impedance tomography. J Med Eng Technol 21:201–232

Boynton BR, Glass G, Frantz ID III, Fredberg JJ (1989) Rib cage vs. abdominal displacement in dogs during forced oscillation to 32 Hz. J Appl Physiol 67:1472–1478

Brazelton TB, Watson KF, Thompson JE, Arnold JH (1999a) Bench validation of respiratory inductive plethysmography in determining the end-expiratory lung volume during high frequency ventilation. Pediatr Res 45:37A [abstract]

Brazelton TB, Watson KF, Thompson JE, Arnold JH (1999b) Respiratory inductive plethysmography is stable during high frequency ventilation. Pediatr Res 45:38A [abstract]

Brazelton TB III, Watson KF, Murphy M, Al Khadra E, Thompson JE, Arnold JH (2001) Identification of optimal lung volume during high-frequency oscillatory ventilation using respiratory inductive plethysmography. Crit Care Med 29:2349–2359

Brismar B, Hedenstierna G, Lundquist H, Strandberg A, Svensson L, Tokics L (1985) Pulmonary densities during anesthesia with muscular relaxation–a proposal of atelectasis. Anesthesiology 62:422–428

Brooks LJ, DiFiore JM, Martin RJ, The CHIME Study Group (1997) Assessment of tidal volume over time in preterm infants using respiratory inductance plethysmography. Pediatr Pulmonol 23:429–433

Brown BH (2003) Electrical impedance tomography (EIT): a review. J Med Eng Technol 27:97–108

Brown K, Aun C, Jackson E, Mackersie A, Hatch D, Stocks J (1998) Validation of respiratory inductive plethysmography using the qualitative diagnostic calibration method in anaesthetized infants. Eur Respir J 12:935–943

Brown BH, Primhak RA, Smallwood RH, Milnes P, Narracott AJ, Jackson MJ (2002a) Neonatal lungs–can absolute lung resistivity be determined non-invasively? Med Biol Eng Comput 40:388–394

Brown BH, Primhak RA, Smallwood RH, Milnes P, Narracott AJ, Jackson MJ (2002b) Neonatal lungs: maturational changes in lung resistivity spectra. Med Biol Eng Comput 40:506–511

Caironi P, Cressoni M, Chiumello D, Ranieri M, Quintel M, Russo SG, Cornejo R, Bugedo G, Carlesso E, Russo R, Caspani L, Gattinoni L (2010) Lung opening and closing during ventilation of acute respiratory distress syndrome. Am J Respir Crit Care Med 181:578–586

Carry PY, Baconnier P, Eberhard A, Cotte P, Benchetrit G (1997) Evaluation of respiratory inductive plethysmography: accuracy for analysis of respiratory waveforms. Chest 111:910–915

Choong K, Chatrkaw P, Frndova H, Cox PN (2003) Comparison of loss in lung volume with open versus in-line catheter endotracheal suctioning. Pediatr Crit Care Med 4:69–73

Constantin JM, Futier E, Cherprenet al, Chanques G, Guerin R, Cayot-Constantin S, Jabaudon M, Perbet S, Chartier C, Jung B, Guelon D, Jaber S, Bazin JE (2010) A recruitment maneuver increases oxygenation after intubation of hypoxemic intensive care unit patients: a randomized controlled study. Crit Care 14:R76

Copnell B, Dargaville PA, Ryan EM, Kiraly NJ, Chin LO, Mills JF, Tingay DG (2009) The effect of suction method, catheter size and suction pressure on lung volume changes during endotracheal suction in piglets. Pediatr Res 66:405–410

Costa EL, Lima RG, Amato MB (2009) Electrical impedance tomography. Curr Opin Crit Care 15:18–24

Costa EL, Musch G, Winkler T, Schroeder T, Harris RS, Jones HA, Venegas JG, Vidal Melo MF (2010) Mild endotoxemia during mechanical ventilation produces spatially heterogeneous pulmonary neutrophilic inflammation in sheep. Anesthesiology 112:658–669

Courtney SE, Pyon KH, Saslow JG, Arnold GK, Pandit PB, Habib RH (2001) Lung recruitment and breathing pattern during variable versus continuous flow nasal continuous positive airway pressure in premature infants: an evaluation of three devices. Pediatrics 107:304–308

Crotti S, Mascheroni D, Caironi P, Pelosi P, Ronzoni G, Mondino M, Marini JJ, Gattinoni L (2001) Recruitment and derecruitment during acute respiratory failure: a clinical study. Am J Respir Crit Care Med 164: 131–140

De Jaegere A, van Veenendaal MB, Michiels A, van Kaam AH (2006) Lung recruitment using oxygenation during open lung high-frequency ventilation in preterm infants. Am J Respir Crit Care Med 174:639–645

Dolfin T, Duffty P, Wilkes DL, Bryan MH (1982) Calibration of respiratory induction plethysmography (Respitrace) in infants. Am Rev Respir Dis 126:577–579

Duffty P, Spriet L, Bryan MH, Bryan AC (1981) Respiratory induction plethysmography (Respitrace): an evaluation of its use in the infant. Am Rev Respir Dis 123:542–546

Dunlop S, Hough J, Riedel T, Fraser JF, Dunster K, Schibler A (2006) Electrical impedance tomography in extremely prematurely born infants and during high frequency oscillatory ventilation analyzed in the frequency domain. Physiol Meas 27:1151–1165

Eberle B, Weiler N, Markstaller K, Kauczor H, Deninger A, Ebert M, Grossmann T, Heil W, Lauer LO, Roberts TP, Schreiber WG, Surkau R, Dick WF, Otten EW, Thelen M (1999) Analysis of intrapulmonary O(2) concentration by MR imaging of inhaled hyperpolarized helium-3. J Appl Physiol 87:2043–2052

Elgellab A, Riou Y, Abbazine A, Truffert P, Matran R, Lequien P, Storme L (2001) Effects of nasal continuous positive airway pressure (NCPAP) on breathing pattern in spontaneously breathing premature newborn infants. Intensive Care Med 27:1782–1787

Erlandsson K, Odenstedt H, Lundin S, Stenqvist O (2006) Positive end-expiratory pressure optimization using electric impedance tomography in morbidly obese patients during laparoscopic gastric bypass surgery. Acta Anaesthesiol Scand 50:833–839

Frerichs I (2000) Electrical impedance tomography (EIT) in applications related to lung and ventilation: a review of experimental and clinical activities. Physiol Meas 21:R1–R21

Frerichs I, Hahn G, Hellige G (1999a) Thoracic electrical impedance tomographic measurements during volume

controlled ventilation-effects of tidal volume and positive end-expiratory pressure. IEEE Trans Med Imaging 18:764–773

Frerichs I, Hahn G, Schiffmann H, Berger C, Hellige G (1999b) Monitoring regional lung ventilation by functional electrical impedance tomography during assisted ventilation. Ann N Y Acad Sci 873:493–505

Frerichs I, Schiffmann H, Hahn G, Hellige G (2001a) Non-invasive radiation-free monitoring of regional lung ventilation in critically ill infants. Intensive Care Med 27:1385–1394

Frerichs I, Dudykevych T, Hinz J, Bodenstein M, Hahn G, Hellige G (2001b) Gravity effects on regional lung ventilation determined by functional EIT during parabolic flights. J Appl Physiol 91:39–50

Frerichs I, Hinz J, Herrmann P, Weisser G, Hahn G, Dudykevych T, Quintel M, Hellige G (2002) Detection of local lung air content by electrical impedance tomography compared with electron beam CT. J Appl Physiol 93:660–666

Frerichs I, Dargaville PA, Dudykevych T, Rimensberger PC (2003a) Electrical impedance tomography: a method for monitoring regional lung aeration and tidal volume distribution? Intensive Care Med 29:2312–2316

Frerichs I, Schiffmann H, Oehler R, Dudykevych T, Hahn G, Hinz J, Hellige G (2003b) Distribution of lung ventilation in spontaneously breathing neonates lying in different body positions. Intensive Care Med 29:787–794

Frerichs I, Pulletz S, Elke G, Reifferscheid F, Schadler D, Scholz J, Weiler N (2009) Assessment of changes in distribution of lung perfusion by electrical impedance tomography. Respiration 77:282–291

Froese AB (1997) High-frequency oscillatory ventilation for adult respiratory distress syndrome: let's get it right this time! Crit Care Med 25:906–908

Gattinoni L, Mascheroni D, Torresin A, Marcolin R, Fumagalli R, Vesconi S, Rossi GP, Rossi F, Baglioni S, Bassi F (1986) Morphological response to positive end expiratory pressure in acute respiratory failure. Computerized tomography study. Intensive Care Med 12:137–142

Gattinoni L, D'Andrea L, Pelosi P, Vitale G, Pesenti A, Fumagalli R (1993) Regional effects and mechanism of positive end-expiratory pressure in early adult respiratory distress syndrome. JAMA 269:2122–2127

Gattinoni L, Caironi P, Pelosi P, Goodman LR (2001) What has computed tomography taught us about the acute respiratory distress syndrome? Am J Respir Crit Care Med 164:1701–1711

Gattinoni L, Caironi P, Cressoni M, Chiumello D, Ranieri VM, Quintel M, Russo S, Patroniti N, Cornejo R, Bugedo G (2006) Lung recruitment in patients with the acute respiratory distress syndrome. N Engl J Med 354:1775–1786

Geddes LA, Baker LE (1967) The specific resistance of biological material-a compendium of data for the biomedical engineer and physiologist. Med Biol Eng 5:271–293

Gerstmann DR, Fouke JM, Winter DC, Taylor AF, deLemos RA (1990) Proximal, tracheal, and alveolar pressures during high-frequency oscillatory ventilation in a normal rabbit model. Pediatr Res 28:367–373

Gothberg S, Parker TA, Griebel J, Abman SH, Kinsella JP (2001) Lung volume recruitment in lambs during high-frequency oscillatory ventilation using respiratory inductive plethysmography. Pediatr Res 49:38–44

Guslits BG, Gaston SE, Bryan MH, England SJ, Bryan AC (1987) Diaphragmatic work of breathing in premature human infants. J Appl Physiol 62: 1410–1415

Habib RH, Pyon KH, Courtney SE (2002) Optimal high-frequency oscillatory ventilation settings by nonlinear lung mechanics analysis. Am J Respir Crit Care Med 166:950–953

Hahn G, Sipinkova I, Baisch F, Hellige G (1995) Changes in the thoracic impedance distribution under different ventilatory conditions. Physiol Meas 16:A161–A173

Harris ND, Suggett AJ, Barber DC, Brown BH (1987) Applications of applied potential tomography (APT) in respiratory medicine. Clin Phys Physiol Meas 8(Suppl A):155–165

Heinrich S, Schiffmann H, Frerichs A, Klockgether-Radke A, Frerichs I (2006) Body and head position effects on regional lung ventilation in infants: an electrical impedance tomography study. Intensive Care Med 32:1392–1398

Henderson RP, Webster JG (1978) An impedance camera for spatially specific measurements of the thorax. IEEE Trans Biomed Eng 25:250–254

Hickling KG (2001) Best compliance during a decremental, but not incremental, positive end-expiratory pressure trial is related to open-lung positive end-expiratory pressure: a mathematical model of acute respiratory distress syndrome lungs. Am J Respir Crit Care Med 163:69–78

Hinz J, Hahn G, Neumann P, Sydow M, Mohrenweiser P, Hellige G, Burchardi H (2003a) End-expiratory lung impedance change enables bedside monitoring of end-expiratory lung volume change. Intensive Care Med 29:37–43

Hinz J, Neumann P, Dudykevych T, Andersson LG, Wrigge H, Burchardi H, Hedenstierna G (2003b) Regional ventilation by electrical impedance tomography: a comparison with ventilation scintigraphy in pigs. Chest 124:314–322

Hinz J, Gehoff A, Moerer O, Frerichs I, Hahn G, Hellige G, Quintel M (2007) Regional filling characteristics of the lungs in mechanically ventilated patients with acute lung injury. Eur J Anaesthesiol 24:414–424

Hoellering AB, Copnell B, Dargaville PA, Mills JF, Morley CJ, Tingay DG (2008) Lung volume and cardiorespiratory changes during open and closed endotracheal suction in ventilated newborn infants. Arch Dis Child Fetal Neonatal Ed 93:F436–F441

Kirpalani H, Abubakar K, Nahmias C, deSa D, Coates G, Schmidt B (1997) [18F]fluorodeoxyglucose uptake in

neonatal acute lung injury measured by positron emission tomography. Pediatr Res 41:892–896
Kneyber MC, van Heerde M, Twisk JW, Plotz FB, Markhors DG (2009) Heliox reduces respiratory system resistance in respiratory syncytial virus induced respiratory failure. Crit Care 13:R71
Konno K, Mead J (1967) Measurement of the separate volume changes of rib cage and abdomen during breathing. J Appl Physiol 22:407–422
Kunst PW, Vonk Noordegraaf A, Hoekstra OS, Postmus PE, de Vries PM (1998) Ventilation and perfusion imaging by electrical impedance tomography: a comparison with radionuclide scanning. Physiol Meas 19:481–490
Lachmann B (1992) Open up the lung and keep the lung open. Intensive Care Med 18:319–321
Landon C (2002) Respiratory monitoring: advantages of inductive plethysmography over impedance pneumography.1–7. http://www.aastweb.org/resources/focusgroups/2003respiratorymonitoring.pdf
Lu Q, Constantin JM, Nieszkowska A, Elman M, Vieira S, Rouby JJ (2006) Measurement of alveolar derecruitment in patients with acute lung injury: computerized tomography versus pressure-volume curve. Crit Care 10:R95
Markhorst DG, van Genderingen HR (2004) Accuracy of respiratory inductive plethysmography in estimating lung volume changes. Crit Care Med 32:1241–1242
Markhorst DG, Jansen JR, van Vught AJ, van Genderingen HR (2005) Breath-to-breath analysis of abdominal and rib cage motion in surfactant-depleted piglets during high-frequency oscillatory ventilation. Intensive Care Med 31:424–430
Markhorst DG, Van Gestel JP, van Genderingen HR, Haitsma JJ, Lachmann B, van Vught AJ (2006) Respiratory inductive plethysmography accuracy at varying PEEP levels and degrees of acute lung injury. J Med Eng Technol 30:166–175
Martinot-Lagarde P, Sartene R, Mathieu M, Durand G (1988) What does inductance plethysmography really measure? J Appl Physiol 64:1749–1756
Mayo JR, MacKay AL, Whittall KP, Baile EM, Pare PD (1995) Measurement of lung water content and pleural pressure gradient with magnetic resonance imaging. J Thorac Imaging 10:73–81
Mayo JR, Aldrich J, Muller NL (2003) Radiation exposure at chest CT: a statement of the Fleischner Society. Radiology 228:15–21
Meier T, Luepschen H, Karsten J, Leibecke T, Grossherr M, Gehring H, Leonhardt S (2008) Assessment of regional lung recruitment and derecruitment during a PEEP trial based on electrical impedance tomography. Intensive Care Med 34:543–550
Monkman SL, Andersen CC, Nahmias C, Ghaffer H, Bourgeois JM, Roberts RS, Schmidt B, Kirpalani HM (2004) Positive end-expiratory pressure above lower inflection point minimizes influx of activated neutrophils into lung. Crit Care Med 32:2471–2475
Morel DR, Forster A, Suter PM (1983) Noninvasive ventilatory monitoring with bellows pneumographs in supine subjects. J Appl Physiol 55:598–606
Morucci JP, Marsili PM (1996) Bioelectrical impedance techniques in medicine. Part III: impedance imaging. Second section: reconstruction algorithms. Crit Rev Biomed Eng 24:599–654
Musante G, Schulze A, Gerhardt T, Everett R, Claure N, Schaller P, Bancalari E (2001) Proportional assist ventilation decreases thoracoabdominal asynchrony and chest wall distortion in preterm infants. Pediatr Res 49:175–180
Neumann P, Zinserling J, Haase C, Sydow M, Burchardi H (1998) Evaluation of respiratory inductive plethysmography in controlled ventilation: measurement of tidal volume and PEEP-induced changes of end-expiratory lung volume. Chest 113:443–451
Pellicano A, Tingay DG, Mills JF, Fasulakis S, Morley CJ, Dargaville PA (2009) Comparison of four methods of lung volume recruitment during high frequency oscillatory ventilation. Intensive Care Med 35: 1990–1998
Pelosi P, D'Andrea L, Vitale G, Pesenti A, Gattinoni L (1994) Vertical gradient of regional lung inflation in adult respiratory distress syndrome. Am J Respir Crit Care Med 149:8–13
Pelosi P, Caironi P, Gattinoni L (2001a) Pulmonary and extrapulmonary forms of acute respiratory distress syndrome. Semin Respir Crit Care Med 22: 259–268
Pelosi P, Goldner M, McKibben A, Adams A, Eccher G, Caironi P, Losappio S, Gattinoni L, Marini JJ (2001b) Recruitment and derecruitment during acute respiratory failure: an experimental study. Am J Respir Crit Care Med 164:122–130
Pelosi P, D'Onofrio D, Chiumello D, Paolo S, Chiara G, Capelozzi VL, Barbas CS, Chiaranda M, Gattinoni L (2003) Pulmonary and extrapulmonary acute respiratory distress syndrome are different. Eur Respir J Suppl 42:48s–56s
Poole KA, Thompson JR, Hallnan HM, Beardsmore CS (2000) Respiratory inductance plethysmography in healthy infants: a comparison of three calibration methods. Eur Respir J 16:1084–1090
Pulletz S, Elke G, Zick G, Schadler D, Scholz J, Weiler N, Frerichs I (2008) Performance of electrical impedance tomography in detecting regional tidal volumes during one-lung ventilation. Acta Anaesthesiol Scand 52:1131–1139
Puybasset L, Gusman P, Muller JC, Cluzel P, Coriat P, Rouby JJ (2000) Regional distribution of gas and tissue in acute respiratory distress syndrome. III. Consequences for the effects of positive end-expiratory pressure. CT Scan ARDS Study Group. Adult Respiratory Distress Syndrome. Intensive Care Med 26:1215–1227
Richard JC, Decailliot F, Janier M, Annat G, Guerin C (2002) Effects of positive end-expiratory pressure and body position on pulmonary blood flow redistribution in mechanically ventilated normal pigs. Chest 122:998–1005
Richard JC, Pouzot C, Gros A, Tourevieille C, Lebars D, Lavenne F, Frerichs I, Guerin C (2009) Electrical

impedance tomography compared to positron emission tomography for the measurement of regional lung ventilation: an experimental study. Crit Care 13:R82

Riedel T, Kyburz M, Latzin P, Thamrin C, Frey U (2009) Regional and overall ventilation inhomogeneities in preterm and term-born infants. Intensive Care Med 35:144–151

Rimensberger PC, Cox PN, Frndova H, Bryan AC (1999a) The open lung during small tidal volume ventilation: concepts of recruitment and "optimal" positive end-expiratory pressure. Crit Care Med 27:1946–1952

Rimensberger PC, Pristine G, Mullen BM, Cox PN, Slutsky AS (1999b) Lung recruitment during small tidal volume ventilation allows minimal positive end-expiratory pressure without augmenting lung injury. Crit Care Med 27:1940–1945

Rimensberger PC, Pache JC, McKerlie C, Frndova H, Cox PN (2000a) Lung recruitment and lung volume maintenance: a strategy for improving oxygenation and preventing lung injury during both conventional mechanical ventilation and high-frequency oscillation. Intensive Care Med 26:745–755

Rimensberger PC, Beghetti M, Hanquinet S, Berner M (2000b) First intention high-frequency oscillation with early lung volume optimization improves pulmonary outcome in very low birth weight infants with respiratory distress syndrome. Pediatrics 105:1202–1208

Roske K, Foitzik B, Wauer RR, Schmalisch G (1998) Accuracy of volume measurements in mechanically ventilated newborns: a comparative study of commercial devices. J Clin Monit Comput 14:413–420

Rudolph A, Markstaller K, Gast KK, David M, Schreiber WG, Eberle B (2009) Visualization of alveolar recruitment in a porcine model of unilateral lung lavage using 3He-MRI. Acta Anaesthesiol Scand 53:1310–1316

Saari AF, Rossing TH, Solway J, Drazen JM (1984) Lung inflation during high-frequency ventilation. Am Rev Respir Dis 129:333–336

Sackner MA, Watson H, Belsito AS, Feinerman D, Suarez M, Gonzalez G, Bizousky F, Krieger B (1989) Calibration of respiratory inductive plethysmograph during natural breathing. J Appl Physiol 66:410–420

Scalfaro P, Pillow JJ, Sly PD, Cotting J (2001) Reliable tidal volume estimates at the airway opening with an infant monitor during high-frequency oscillatory ventilation. Crit Care Med 29:1925–1930

Schibler A, Yuill M, Parsley C, Pham T, Gilshenan K, Dakin C (2009) Regional ventilation distribution in non-sedated spontaneously breathing newborns and adults is not different. Pediatr Pulmonol 44: 851–858

Schmidt HC, Tsay DG, Higgins CB (1986) Pulmonary edema: an MR study of permeability and hydrostatic types in animals. Radiology 158:297–302

Schulze A, Suguihara C, Gerhardt T, Schaller P, Claure N, Everett R, Devia C, Hehre D, Bancalari E (2001) Inductance plethysmography: an alternative signal to servocontrol the airway pressure during proportional assist ventilation in small animals. Pediatr Res 49:169–174

Schuster DP, Howard DK (1994) The effect of positive end-expiratory pressure on regional pulmonary perfusion during acute lung injury. J Crit Care 9:100–110

Seagar AD, Barber DC, Brown BH (1987) Theoretical limits to sensitivity and resolution in impedance imaging. Clin Phys Physiol Meas 8(Suppl A):13–31

Serrano RE, de LB, Casas O, Feixas T, Calaf N, Camacho V, Carrio I, Casan P, Sanchis J, Riu PJ (2002) Use of electrical impedance tomography (EIT) for the assessment of unilateral pulmonary function. Physiol Meas 23:211–220

Smallwood RH, Hampshire AR, Brown BH, Primhak RA, Marven S, Nopp P (1999) A comparison of neonatal and adult lung impedances derived from EIT images. Physiol Meas 20:401–413

Stefano JL, Spitzer AR, Baumgart S, Davis JM, Fox WW (1986) Inductive plethysmography–a facilitated postural calibration technique for rapid and accurate tidal volume determination in low birth weight premature newborns. Am Rev Respir Dis 134:1020–1024

Strömberg NOT, Dahlbäck GO, Gustafsson PM (1993) Evaluation of various models for respiratory inductance plethysmography calibration. J Appl Physiol 74:1206–1211

Tabachnik E, Muller N, Toye B, Levison H (1981) Measurement of ventilation in children using the respiratory inductive plethysmograph. J Pediatr 99:899

Tingay DG (2013) Indicators of optimal lung volume during high-frequency oscillatory ventilation in infants. Crit Care Med 41:237–244

Tingay DG, Mills JF, Pellicano A, Morley CJ, Dargaville PA (2005) Time to stabilise lung volume after changing mean airway pressure during high frequency oscillatory ventilation (HFOV). Pediatr Res 57(Suppl):A2044 [abstract]

Tingay DG, Mills JF, Morley CJ, Pellicano A, Dargaville PA (2006) The deflation limb of the pressure-volume relationship in infants during high-frequency ventilation. Am J Respir Crit Care Med 173:414–420

Tingay DG, Copnell B, Mills JF, Morley CJ, Dargaville PA (2007a) Effects of open endotracheal suction on lung volume in infants receiving HFOV. Intensive Care Med 33:689–693

Tingay DG, Mills JF, Morley CJ, Pellicano A, Dargaville PA (2007b) Trends in use and outcome of newborn infants treated with high frequency ventilation in Australia and New Zealand, 1996–2003. J Paediatr Child Health 43:160–166

Valta P, Takala J, Foster R, Weissman C, Kinney JM (1992a) Evaluation of respiratory inductive plethysmography in the measurement of breathing pattern and PEEP-induced changes in lung volume. Chest 102:234–238

Valta P, Takala J, Eissa NT, Milic-Emili J (1992b) Effects of PEEP on respiratory mechanics after open heart surgery. Chest 102:227–233

van Kaam AH, Rimensberger PC (2007) Lung-protective ventilation strategies in neonatology: what do we know–what do we need to know? Crit Care Med 35:925–931

van Kaam AH, De Jaegere A, Haitsma JJ, van Aalderen WM, Kok JH, Lachmann B (2003) Positive pressure ventilation with the open lung concept optimizes gas exchange and reduces ventilator-induced lung injury in newborn piglets. Pediatr Res 53:245–253

van Kaam AH, Haitsma JJ, De Jaegere A, van Aalderen WM, Kok JH, Lachmann B (2004a) Open lung ventilation improves gas exchange and attenuates secondary lung injury in a piglet model of meconium aspiration. Crit Care Med 32:443–449

van Kaam AH, Haitsma JJ, Dik WA, Naber BA, Alblas EH, De Jaegere A, Kok JH, Lachmann B (2004b) Response to exogenous surfactant is different during open lung and conventional ventilation. Crit Care Med 32:774–780

Vazquez de Anda GF, Hartog A, Verbrugge SJ, Gommers D, Lachmann B (1999) The open lung concept: pressure-controlled ventilation is as effective as high-frequency oscillatory ventilation in improving gas exchange and lung mechanics in surfactant-deficient animals. Intensive Care Med 25:990–996

Vazquez de Anda GF, Gommers D, Verbrugge SJ, De Jaegere A, Lachmann B (2000) Mechanical ventilation with high positive end-expiratory pressure and small driving pressure amplitude is as effective as high-frequency oscillatory ventilation to preserve the function of exogenous surfactant in lung-lavaged rats. Crit Care Med 28:2921–2925

Venegas JG, Harris RS, Simon BA (1998) A comprehensive equation for the pulmonary pressure-volume curve. J Appl Physiol 84:389–395

Viard R, Tourneux P, Storme L, Girard JM, Betrouni N, Rousseau J (2008) Magnetic resonance imaging spatial and time study of lung water content in newborn lamb: methods and preliminary results. Invest Radiol 43:470–480

Victorino JA, Borges JB, Okamoto VN, Matos GF, Tucci MR, Caramez MP, Tanaka H, Sipmann FS, Santos DC, Barbas CS, Carvalho CR, Amato MB (2004) Imbalances in regional lung ventilation: a validation study on electrical impedance tomography. Am J Respir Crit Care Med 169:791–800

Vieira SR, Puybasset L, Richecoeur J, Lu Q, Cluzel P, Gusman PB, Coriat P, Rouby JJ (1998) A lung computed tomographic assessment of positive end-expiratory pressure-induced lung overdistension. Am J Respir Crit Care Med 158:1571–1577

Watson HL, Poole DA, Sackner MA (1988) Accuracy of respiratory inductive plethysmographic cross-sectional areas. J Appl Physiol 65:306–308

Weber K, Courtney SE, Pyon KH, Chang GY, Pandit PB, Habib RH (2000) Detecting lung overdistention in newborns treated with high-frequency oscillatory ventilation. J Appl Physiol 89:364–372

Weese-Mayer DE, Corwin MJ, Peuker MR, DiFiore JM, Hufford DR, Tinsley LR, Neuman MR, Martin RJ, Brooks LJ, Davidson Ward SL, Lister G, Willinger M, The CHIME Study Group (2000) Comparison of apnea identified by respiratory inductance plethysmography with that detected by end-tidal CO2 or thermistor. Am J Respir Crit Care Med 162:471–480

Werchowski JL, Sanders MH, Costantino JP, Sciurba FC, Rogers RM (1990) Inductance plethysmography measurement of CPAP-induced changes in end-expiratory lung volume. J Appl Physiol 68:1732–1738

Wolf GK, Grychtol B, Frerichs I, van Genderingen HR, Zurakowski D, Thompson JE, Arnold JH (2007) Regional lung volume changes in children with acute respiratory distress syndrome during a derecruitment maneuver. Crit Care Med 35:1972–1978

Wrigge H, Zinserling J, Muders T, Varelmann D, Gunther U, von der Groeben C, Magnusson A, Hedenstierna G, Putensen C (2008) Electrical impedance tomography compared with thoracic computed tomography during a slow inflation maneuver in experimental models of lung injury. Crit Care Med 36:903–909

Zhao Z, Moller K, Steinmann D, Frerichs I, Guttmann J (2009) Evaluation of an electrical impedance tomography-based global inhomogeneity index for pulmonary ventilation distribution. Intensive Care Med 35:1900–1906

Zimova-Herknerova M, Plavka R (2006) Expired tidal volumes measured by hot-wire anemometer during high-frequency oscillation in preterm infants. Pediatr Pulmonol 41:428–433